Taylor & Francis
Taylor & Francis Group

Philosophical Magazine

ISSN: 1478-6435 (Print) 1478-6443 (Online) Journal homepage: https://www.tandfonline.com/loi/tphm20

# Long-range chemical interactions in solid-state reactions: effect of an inert Ag interlayer on the formation of $L1_0$-FePd in epitaxial Pd(0 0 1)/Ag(0 0 1)/Fe(0 0 1) and Fe(0 0 1)/Ag(0 0 1)/Pd(0 0 1) trilayers

**Victor Myagkov, Oleg Bayukov, Yurii Mikhlin, Victor Zhigalov, Liudmila Bykova & Galina Bondarenko**

**To cite this article:** Victor Myagkov, Oleg Bayukov, Yurii Mikhlin, Victor Zhigalov, Liudmila Bykova & Galina Bondarenko (2014) Long-range chemical interactions in solid-state reactions: effect of an inert Ag interlayer on the formation of $L1_0$-FePd in epitaxial Pd(001)/Ag(001)/Fe(001) and Fe(001)/Ag(001)/Pd(001) trilayers, Philosophical Magazine, 94:23, 2595-2622, DOI: 10.1080/14786435.2014.926037

**To link to this article:** https://doi.org/10.1080/14786435.2014.926037

*Philosophical Magazine*, 2014
Vol. 94, No. 23, 2595–2622, http://dx.doi.org/10.1080/14786435.2014.926037

Taylor & Francis
Taylor & Francis Group

# Long-range chemical interactions in solid-state reactions: effect of an inert Ag interlayer on the formation of $L1_0$-FePd in epitaxial Pd(0 0 1)/Ag(0 0 1)/Fe(0 0 1) and Fe(0 0 1)/Ag(0 0 1)/Pd(0 0 1) trilayers

Victor Myagkov[a]*, Oleg Bayukov[a], Yurii Mikhlin[b], Victor Zhigalov[a], Liudmila Bykova[a] and Galina Bondarenko[b]

[a]*Kirensky Institute of Physics, Russian Academy of Sciences, Siberian Branch, Krasnoyarsk 660036, Russia;* [b]*Institute of Chemistry and Chemical Technology, Russian Academy of Sciences, Siberian Branch, Krasnoyarsk 660049, Russia*

(*Received 18 December 2013; accepted 13 May 2014*)

The effect of 0, 0.5, and 1 μm-thick Ag interlayers on the chemical interaction between Pd and Fe in epitaxial Pd(0 0 1)/Ag(0 0 1)/Fe(0 0 1)/MgO(0 0 1) and Fe(0 0 1)/Ag(0 0 1)/Pd(0 0 1)/MgO(0 0 1) trilayers has been studied using X-ray diffraction, $^{57}$Fe Mössbauer spectroscopy, X-ray photoelectron spectroscopy, and magnetic structural measurements. No mixing of Pd and Fe occurs via the chemically inert Ag layer at annealing temperatures up to 400 °C. As the annealing temperature is increased above 400 °C, a solid-state synthesis of an ordered $L1_0$-FePd phase begins in the Pd(0 0 1)/Ag(0 0 1)/Fe(0 0 1) and Fe(0 0 1)/Ag(0 0 1)/Pd(0 0 1) film trilayers regardless of the thickness of the buffer Ag layer. In all samples, annealing above 500 °C leads to the formation of a disordered $Fe_xPd_{1-x}$(0 0 1) phase; however, in samples lacking the Ag layer, the synthesis of $Fe_xPd_{1-x}$ is preceded by the formation of an ordered $L1_2$-$FePd_3$ phase. An analysis of the X-ray photoelectron spectroscopy results shows that Pd is the dominant moving species in the reaction between Pd and Fe. According to the preliminary results, the 2.2 μm-thick Ag film does not prevent the synthesis of the $L1_0$-FePd phase and only slightly increases the phase's initiation temperature. Data showing the ultra-fast transport of Pd atoms via thick inert Ag layers are interpreted as direct evidence of the long-range character of the chemical interaction between Pd and Fe. Thus, in the reaction state, Pd and Fe interact chemically even though the distance between them is about $10^4$ times greater than an ordinary chemical bond length.

**Keywords:** Fe–Pd system; epitaxial thin film; inert Ag buffer layer; diffusion; solid-state reactions; $L1_0$; long-range chemical interactions

**PACS:** 68.35.Dv, 68.35.Fx, 66.30.Ny, 66.30.Pa, 81.20

## 1. Introduction

Diffusion is one of the unique phenomena that control major natural processes. It is a basic contributor to chemical reactions and structural transformations in solids [1,2]. Solid-state reactions, including those occurring in thin films and multilayers, comprise three successive stages: (1) breakage of reagent chemical bonds, (2) diffusion transfer

*Corresponding author. Email: miagkov@iph.krasn.ru

of reagent atoms via a reaction product, and (3) rearrangement and formation of new bonds. The reaction rate is determined by step 2, which is the primary stage.

Traditionally, solid-state migration of reacting atoms via a layer of reaction product is based on defect-mediated diffusion, which leads to their random walk over a crystal lattice. The mean distance d that an atom moves over time $t$ equals the mean-square atomic displacement $\langle \Delta x^2 \rangle$ and satisfies the Einstein equation $d = \langle \Delta x^2 \rangle = 2Dt$. In numerous studies on solid-state reactions in thin films and multilayers, the parabolic growth of the reaction layer thickness d which satisfies the Einstein equation is presented as experimental proof of the diffusive nature of the reaction. However, at the initial stage, the thickness of a reaction product layer often grows in proportion to time, and only in the last stage the reaction kinetic becomes parabolic [3,4].

A unique characteristic of solid-state reactions in thin films is the formation of a single phase (*first phase*) on the interface between the reacting layers at the so-called initiation temperature, $T_0$. As the annealing temperature is increased, other phases can also occur to form the phase sequence. To date, the formation of the first phase and the phase sequence has not been explained, although many models have been proposed. As a rule, these models consider the high-temperature part of the phase diagrams or use thermodynamic arguments [3–8]. Most thin-film solid-state reactions occur at 100–600 °C, [3–7] when diffusion is minor [9,10]. Some reactions, however, have already begun at room temperature [11]. It remains to be understood why solid-state reactions on the nanoscale have low initiation temperatures, while a chemical bond breaks at a melting temperature. It is now universally accepted that diffusion along grain boundaries, dislocations, and other structural defects is a few orders more than bulk diffusion and plays a decisive role in thin-film solid-state reactions [3]. However, this explanation does not take into account the bulk diffusion into the depth of the grain. The nature of atomic migration during the low-temperature solid-state reactions in bilayers and multilayers is as yet unclear. To a large extent, this effect is inconsistent with the diffusion mechanism. The major inconsistencies are the following:

(1) The threshold character of a thin-film solid-state reaction. According to calorimetric and resistance measurements, intense mixing on the interface begins after the initiation temperature $T_0$ is exceeded [12–14]. Meanwhile, the diffusion scenario suggests that the solid-state reactions on the interface between reagents should occur at any temperature, and that the reaction layer thickness depends only on the temperature and annealing time.
(2) Above the initiation temperature ($T > T_0$), 100 nm thick layers often react over the entire depth for a typical annealing time of 1 h. The diffusivity estimated by the Einstein equation is $D \sim 10^{-17}$ m$^2$/s, which agrees with the diffusivity along grain boundaries [3,4]. However, the atomic migration deep in the grains is insignificant, since the diffusivity in films at temperatures 100–400 °C is $D < 10^{-22}$ m$^2$/s [9,10].
(3) In the diffusion reaction mechanism, the break of a chemical bond in the film reagents comprising the bilayers at $T > T_0$ (stage 1) is not related to the further interdiffusion of atoms via a reaction layer (stage 2). However, the layers of the same film reagents separated by a certain distance do not exhibit a break in the atoms' chemical bond or their diffusion from the surface. In other words, the breakage of chemical bonds and mutual atomic migration only occur when reacting layers are

included in the bilayers and multilayers and the temperature exceeds the initiation temperature ($T > T_0$).

(4) Ultrafast atomic transport occurs at the initiation of solid-state reactions in Co/Si [15] and Mo/Si [16] multilayer thin films by femtosecond laser irradiation. In Co/Si and Mo/Si samples, mixing of the layers with thicknesses of ~10 nm occurs for an irradiation time of 150 fs. This corresponds to diffusivity $D \sim (10^{-10}–10^{-8})$ $m^2/s$, which is unrealistic for solid-state diffusion.

It is also difficult to understand the atomic mechanisms for diffusion in other cases, such as in metal glasses [17] in the reactions in Ni–Al laminates under laser-shock loading [18] upon mixing induced by $Ar^+$ ion irradiation in an Ag–Ge bilayer system [19] upon anomalously large mixing in aluminum-transition metal bilayers [20] in the self-sustaining wave reactions in multilayers [21] and at the solid-state transformations initiated by shock waves [22]. These difficulties are magnified since the existence of dominant diffusing species in thin-film reactions remains unexplained [5,23–26].

It is well known that the interatomic interaction potentials that describe chemical bonds have a short range and rapidly decrease at distances greater than the chemical bond length. Therefore, the placement of thin chemically inert layers (diffusion barriers) between the reacting films should suppress a reaction. Most of the studies in this area have attempted to clarify the nature of atomic migration and reactions via thin ($d < 50$ nm) diffusion barriers [27–33]. It has been found that often chemically inert layers do not act as diffusion barriers. Instead, it has been suggested that structural defects (e.g. grain boundaries and dislocations) that occur with increasing annealing temperature are the main cause of failure in diffusion barriers [27,28]. Early studies showed that single-crystal films act as more effective diffusion barriers compared with polycrystalline films [3,27]. A priori, it is accepted that ultra-thick ($d > 50$ nm) chemically inert barriers always prevent a solid-state reaction. For this reason, the effect of such barriers on the kinetics and main characteristics of solid-state reactions have not been systematically studied.

This work focuses on the long-range chemical interactions (LRCIs) in thin-film solid-state reactions. We chose to investigate the solid-state reaction between elemental Fe and Pd film reagents separated by chemically inert Ag layers having thicknesses of 0, 0.5, 1, and 2.2 μm. In recent years, film alloys of Fe and Pd have attracted both fundamental and practical interest. They have unique magnetic and structural properties [34–42] due to the coexistence of disordered $Fe_xPd_{1-x}$ alloys that form a complete range of fcc solid solutions, a chemically ordered $L1_0$-FePd phase with large magnetocrystalline anisotropy constants ($K_1 = (1.7 \pm 0.3) \times 10^6$ J/m$^3$ and $K_2 \sim (1.5 \pm 0.5) \times 10^5$ J/m$^3$), [41] and a magnetically soft $L1_2$-$FePd_3$ phase with a low anisotropy constant ($K_1 = -2.0 \times 10^2$ J/m$^3$) [42]. We present convincing experimental evidence for the formation of the first $L1_0$-FePd phase after annealing at 400 °C and the disordered $Fe_xPd_{1-x}$ solution above 550 °C, regardless of the thickness of a chemically inert Ag barrier. The analysis of atomic migration via micron barriers leads us to the following hypothesis. In contrast to the commonly accepted view of diffusion in thin-film solid-state reactions, we propose that the moving force of atomic migration via inert barriers or a reaction product layer is the LRCIs between reacting atoms.

## 2. Experimental section

The experiments used epitaxial Pd(0 0 1)/Ag(0 0 1)/Fe(0 0 1) and Fe(0 0 1)/Ag(0 0 1)/Pd (0 0 1) films fabricated by the successive deposition of Pd, Ag, Fe, and Fe, Ag, Pd layers, respectively, onto single-crystal MgO(0 0 1) substrates. The Fe, Ag, and Pd layers were deposited at a pressure of $10^{-6}$ mbar and a temperature of 250 °C to ensure the correct orientation of their growth. The thicknesses of the diffusion-inert Ag barrier layers were 0.5 for Fe(0 0 1)/Ag(0 0 1)/Pd(0 0 1)/MgO(0 0 1) and 1 μm for Pd(0 0 1)/Ag(0 0 1)/Fe(0 0 1)/MgO(0 0 1) (hereafter, Fe/Ag(0.5 μm)/Pd and Pd/Ag (1 μm)/Fe, respectively). For comparison, we analysed a reference sample of Pd(0 0 1)/Fe(0 0 1)/MgO(0 0 1) without the interlayer (hereafter, Pd/Fe). The initial samples were annealed under a vacuum of $10^{-6}$ mbar at temperatures from 300 to 700 °C with a pitch of 50 °C for 30 min. To estimate the maximum radius of the chemical interaction, we obtained epitaxial Pd/Ag(0 0 1)/Fe(0 0 1)/MgO(0 0 1) trilayers with a 2.2 μm thick Ag barrier layer (hereafter, Pd/Ag(2.2 μm)/Fe) and annealed them at temperatures from 300 to 700 °C. The thicknesses of the reacting Fe and Pd layers were monitored using a quartz oscillator; in all cases, these thicknesses were 180 and 130 nm, respectively. The forming phases were identified by X-ray diffraction (XRD) ($CuK_\alpha$ radiation). The epitaxial relations between the MgO(0 0 1) substrate, Ag(0 0 1) buffer layer, and reacting Fe(0 0 1) and Pd(0 0 1) layers were investigated on a PANalytikal X'Pert PRO diffractometer that was equipped with a PIXctl detector using $CuK_\alpha$ radiation monochromatized by a secondary graphite monochromator. The chemical composition was determined and the film thicknesses were calibrated using the X-ray fluorescent method.

The in-plane fourfold anisotropy constant $K_4$ was measured by the torque method with a maximum magnetic field of 18 kOe. The in-plane torque curve $L(\varphi)$ was determined as

$$2L(\varphi) = K_4 V \sin 4\varphi + 2K_u V \sin(2\varphi + \gamma), \quad (1)$$

where $K_u$ is the uniaxial anisotropy constant, $V$ is the film volume, $\varphi$ is the angle between the fourfold anisotropy easy axis and the direction of magnetization, and $\gamma$ is the angle between the fourfold anisotropy easy axis and the uniaxial anisotropy. The uniaxial anisotropy is mainly caused by the roughness of the surface of the MgO(0 0 1) substrate. The value of $K_4$ was calculated from the torque curve $L(\varphi)$ at the maximum fourfold harmonic term $2L_{max} = K_4 V$.

Mossbauer measurements were performed on a MS-1104Em spectrometer with a $Co^{57}$(Cr) source. The spectra obtained were identified in two stages. In the first stage, we determined the probability distributions of hyperfine magnetic fields $P(H)$. The maxima and features observed in these $P(H)$ curves indicate the presence of nonequivalent iron positions. We built model spectra based on these data. Subsequently, in the second identification stage, we fit the model spectra to the experimental spectra, varying all the parameters of the hyperfine structure. The chemical isomeric shifts are presented relative to metal α-Fe.

X-ray photoelectron spectra (XPS) were obtained using a SPECS photoelectron spectrometer with a PHOIBOS 150 MCD-9 analyser and a Mg $K_\alpha$ X-ray source (SPECS Surface Nano Analysis GmbH, Germany) at an electron take-off angle of 90°; the pass energy of the analyser was 20 eV for wide scans and 8 eV for narrow scans. The C 1s

peak at 285.0 eV from carbonaceous contamination film was used as a charging reference, and no charging effects were observed. Surface contaminants and oxidized layers were removed by $Ar^+$ ion bombardment using a SPECS PU-IQE 12/38 scanning ion source operating at an ion beam energy and ion current of 2.5 keV and 15 μA, respectively. The relative concentrations of elements were determined by the full-range spectra recorded at a transmission energy of 20 eV, using a PHOIBOS 150 MCD9 hemispherical energy analyser with empirical sensitivity coefficients. All measurements were performed at room temperature.

## 3. Results

### 3.1. *X-ray study*

Figures 1–3 show the XRD patterns for the Pd/Fe, Fe/Ag(0.5 μm)/Pd, and Pd/Ag(1 μm)/Fe samples heated to 700 °C. Apart from the MgO(0 0 2) peaks, the patterns of all as-grown samples contain strong Pd(0 0 2) and Fe(0 0 2) reflections. The samples of Pd/Ag (0.5 μm)/Fe (Figure 2) and Fe/Ag(1 μm)/Pd (Figure 3) also yield strong Ag(0 0 2) and weak Ag(1 1 1) peaks. Using asymmetric scanning of the (1 1 3)Fe, (1 1 3)Pd, and (1 1 3)Ag reflections, as well as the (1 1 3) reflection of the MgO substrate, we determined orientation relationships between the substrate, the reacting Fe and Pd layers,

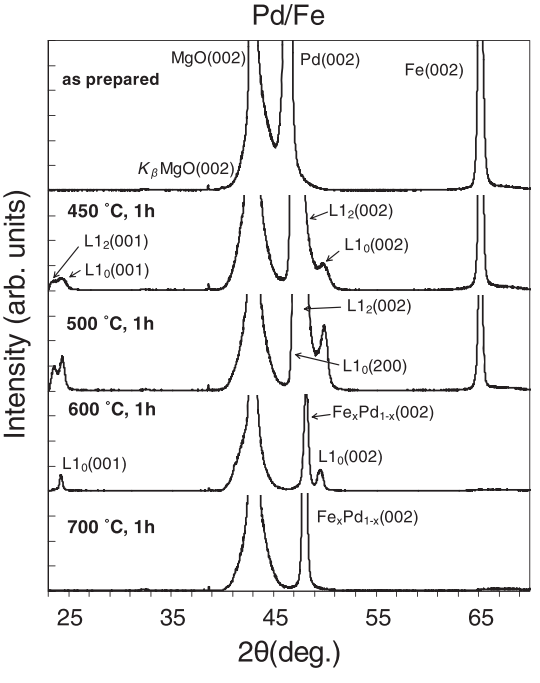


Figure 1. XRD spectra of the Pd/Fe film during the solid-state reaction between Pd and Fe at different annealing temperatures $T_S$. After annealing at 450 °C, the epitaxial ordered $L1_0$-FePd (0 0 1) and $L1_2$-$FePd_3$(0 0 1) phases are synthesized. The reaction completes after annealing at 700 °C with the formation of the disordered $Fe_xPd_{1-x}$(0 0 1) phase.

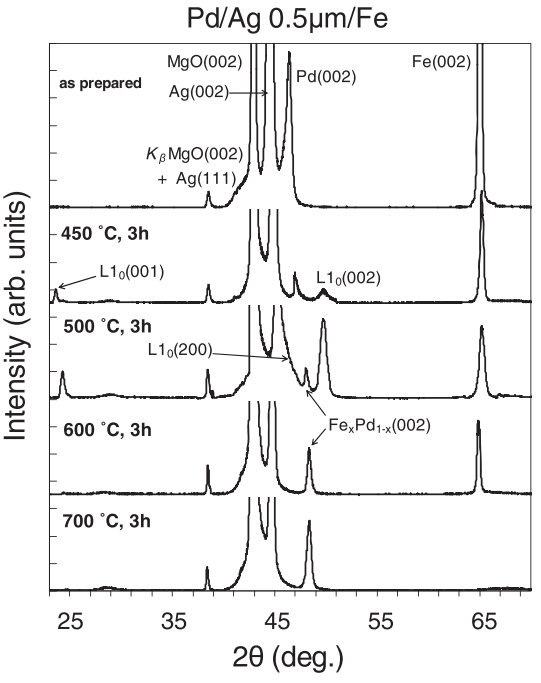


Figure 2. XRD spectra of the Fe/Ag(0.5 μm)/Pd film at different annealing temperatures $T_S$. After annealing at 450 °C, the epitaxial ordered $L1_0$-FePd(0 0 1) phase forms. This result, together with the formation of the disordered $Fe_xPd_{1-x}$(0 0 1) phase, shows that the inert Ag(0.5 μm) buffer layer does not prevent the solid-state reaction between Pd and Fe.

and the inert Ag buffer layers. The Fe(0 0 1), Ag(0 0 1), and Pd(0 0 1) layers epitaxially grow on the MgO(0 0 1) surface according to the following orientation relationships:

$$\begin{aligned}
&\mathrm{Pd}(0\,0\,1)[1\,0\,0]||\mathrm{Fe}(0\,0\,1)[1\,1\,0]||\mathrm{MgO}(0\,0\,1)[1\,0\,0]\ \text{for Pd/Fe},\\
&\mathrm{Fe}(0\,0\,1)[1\,1\,0]||\mathrm{Ag}(0\,0\,1)[1\,0\,0]||\mathrm{Pd}(0\,0\,1)[100]||\mathrm{MgO}(0\,0\,1)[1\,0\,0]\ \text{for}\\
&\mathrm{Fe/Ag}(0.5\,\mu\mathrm{m})/\mathrm{Pd}, \text{and}\\
&\mathrm{Pd}\ (0\,0\,1)[1\,0\,0]||\mathrm{Ag}(0\,0\,1)[1\,0\,0]||\mathrm{Fe}(0\,0\,1)[1\,1\,0]||\\
&\mathrm{MgO}(0\,0\,1)[1\,0\,0]\ \text{for Pd/Ag}(1\,\mu\mathrm{m})/\mathrm{Fe}
\end{aligned} \tag{2}$$

Relationships (2) are consistent with previous data on the epitaxial relationships Fe(0 0 1)[1 1 0]||MgO(0 0 1)[1 0 0] [43] Fe(0 0 1)[1 1 0]||Pd(0 0 1)[1 0 0]||MgO(0 0 1)[1 0 0] [44] and Fe(0 0 1)[1 1 0]||Ag (0 0 1)[1 0 0]||MgO(0 0 1) [45,46]. It should be noted that in all three samples, the Pd(0 0 1) and Ag (0 0 1) layers have a cube-on-cube texture with the MgO(0 0 1) substrate, and only the Fe(0 0 1) lattice is rotated by 45° relative to the MgO (0 0 1) lattice. According to the results of the X-ray studies, annealing of the Pd/Fe, Fe/Ag (0.5 μm)/Pd, and Pd/Ag(1 μm)/Fe samples at temperatures below 400 °C does not lead to the formation of new phases. In all three samples, the solid-state reaction between Pd and Fe began above 400 °C. After annealing at 450 °C, the strong Pd(0 0 2) and Fe(0 0 2)

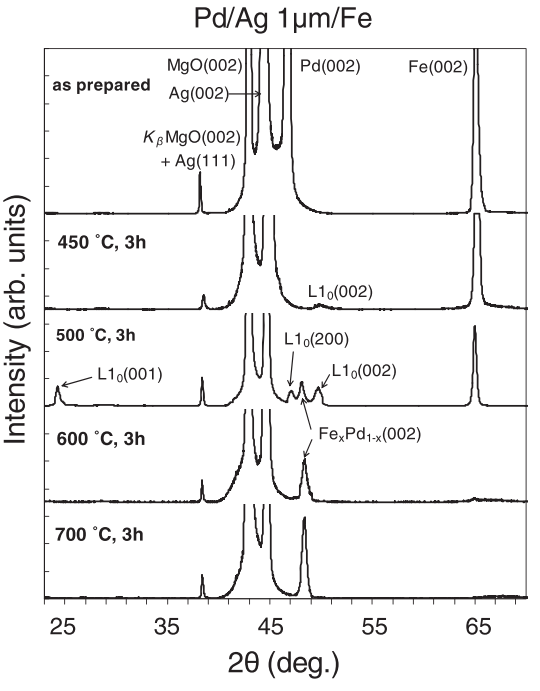


Figure 3. XRD spectra of the Pd/Ag(1 μm)/Fe film at different annealing temperatures $T_S$. The start of the formation of the epitaxial ordered $L1_0$-FePd(0 0 1) phase after annealing at 450 °C and the further synthesis of the disordered $Fe_xPd_{1-x}$(0 0 1) phase after annealing at 700 °C indicate that the inert Ag(1 μm) buffer layer does not suppress the reaction between Pd and Fe.

reflections start to weaken and the new superstructural (0 0 1) and basic (0 0 2) peaks and the (2 0 0) reflection of the ordered $L1_0$-FePd phase occur. For Pd/Fe (without the inert Ag layer), the (0 0 1) and (0 0 2) peaks from the ordered $L1_2$-$FePd_3$ phase also occur, and they persist after annealing at 500 °C (Figure 1). For the samples of Fe/Ag(0.5 μm)/Pd (Figure 2) and Pd/Ag(1 μm)/Fe (Figure 3), no $L1_2$-$FePd_3$ phase was observed at any annealing temperature. Note that the (0 0 2) peak of the unreacted Pd masks the (2 0 0) reflections from the $L1_0$-FePd and $L1_2$-$FePd_3$ phases. Above 500 °C, all samples begin forming the disordered $Fe_xPd_{1-x}$ phase; after annealing at 700 °C, this phase becomes dominant. The (0 0 2)Fe peaks vanish after annealing at 700 °C which indicates a completion of alloying. For all samples, the results of asymmetrical scanning show the only epitaxial relationship

$$(0\,0\,1), [1\,0\,0]\mathrm{Fe}_x\mathrm{Pd}_{1-x} || (0\,0\,1), [1\,0\,0]\mathrm{Mgo}. \tag{3}$$

Using pulsed laser deposition, relationship (3) was observed at the epitaxial growth of $Fe_xPd_{1-x}$ films (19–37 at% Pd) formed on MgO(1 0 0) at room temperature [47].

As shown in [41], in epitaxial film systems of the Fe(0 0 1)/Pd(0 0 1) 1Fe:1Pd atomic composition, the formation of the $L1_0$-FePd local structure is very sensitive to annealing temperature and time. Even at the first synthesis stage of the $L1_0$-FePd phase at 450 °C, the occurrence of the (2 0 0) reflection indicates that the structure of the

reaction product layer contains three types of $L1_0$-FePd crystallites, with the $c$ axes parallel to the three main $\langle 1\,0\,0\rangle$ axes of the MgO substrate. Such a structure is often observed in FePd, CoPt, and FePt alloys [48,49], thin films [50,51], and nanoparticles [52]. As the annealing temperature is increased to 500 °C, the structure is rearranged; from the three types of crystallites, only (0 0 1) $L1_0$ crystallites remain and their fraction becomes dominant after annealing for 10 h. This drastically changes the torque curves: the fourfold in-plane magnetic anisotropy changes for the eightfold in-plane magnetic anisotropy; this is extraordinary for the (0 0 1) $L1_0$ films [41].

The (2 0 0) reflection of the $L1_0$-FePd phase occurs only for Pd/Ag(0.5 μm)/Fe (Figure 2) and Fe/Ag(1 μm)/Pd (Figure 3). The (2 0 0) reflection is not observed for the Pd/Fe sample (Figure 1). This means that in Fe/Ag(0.5 μm)/Pd and Pd/Ag(1 μm)/Fe, a structure with three types of crystallites is formed, while in Pd/Fe there is a preferred texture with the [0 0 1]$L1_0$-FePd direction parallel to the [0 0 1] MgO.

An analysis of the XRD patterns for these samples shows that, regardless of the thickness of the inert Ag buffer layer at a temperature of ~400 °C, the solid-state reaction between Fe and Pd begins with a synthesis of the ordered $L1_0$-FePd phase, which then gradually transforms to the disordered $Fe_xPd_{1-x}$ phase above 500 °C. After annealing at 700 °C, the samples contain no iron or palladium; only the disordered epitaxial $Fe_xPd_{1-x}$ phase remains. Thus, in Fe/Ag(0.5 μm)/Pd and Pd/Ag(1 μm)/Fe, as the annealing temperature increases the phase sequence (~400 °C) $L1_0$-FePd → (~500 °C) $Fe_xPd_{1-x}$ is formed. A feature of the Pd/Fe sample is the presence of $L1_2$-$FePd_3$ in the phase sequence (~400 °C)$L1_0$-FePd, $L1_2$-$FePd_3$ → (~500 °C) $Fe_xPd_{1-x}$. However, the formation of the $L1_2$-$FePd_3$ phase is also present in the Fe/Ag(0.5 μm)/Pd and Pd/Ag (1 μm)/Fe samples.

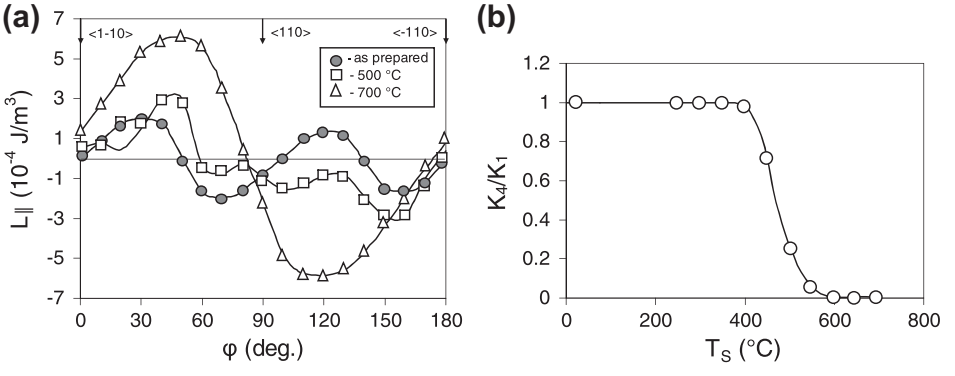


Figure 4. (a) Evolution of the in-plane torque curves $L\|(\varphi)$ (bulk Fe layer) obtained by rotation of a magnetic field from the $\langle 1\,\bar{1}\,0\rangle$ to $\langle 1\,\bar{1}\,0\rangle$ MgO(0 0 1) direction for the Pd/Fe film as a result of the solid-state reaction between Pd and Fe at different annealing temperatures $T_S$. The magnetocrystalline anisotropy constant $K_1 = 5.0 \times 10^4$ J/m$^3$ for the Fe(0 0 1) layer was determined from the torque curves of the as-deposited sample. The formation of the eightfold torque curve at 500 °C is characteristic of the $L1_0$(0 0 1) phase [41]. (b) Relative in-plane fourfold magnetic constant $K_4/K_1$ as a function of annealing temperature $T_S$. The sharp drop of the in-plane fourfold magnetic constant $K_4$ at 700 °C is related to the formation of the disordered magnetically soft $Fe_xPd_{1-x}$ phase [42].

### 3.2. *Anisotropy study*

All the as-grown samples, Pd/Fe (Figure 4(a)), Fe/Ag(0.5 μm)/Pd (Figure 5(a)), and Pd/Ag(1 μm)/Fe (Figure 6(a)), are characterized by a fourfold in-plane anisotropy. The torque curves show that the Pd/Ag(1 μm)/Fe and Pd/Fe samples with the Fe(0 0 1) layer have easy axes that coincide with the [1 1 0] and [1 $\bar{1}$ 0] directions of the MgO(0 0 1). The value of the fourfold anisotropy constant $K_4 = 5.0 \times 10^4$ J/m$^3$ is typical of Fe(0 0 1)/MgO(0 0 1) films fabricated by different methods [43,53–55], and it coincides with the first magnetocrystalline anisotropy constant for bulk iron [56]. In the Fe/Ag(0.5 μm)/Pd sample with the Fe(0 0 1) layer deposited onto the Ag(0 0 1) surface, the anisotropy constant is somewhat smaller, with $K_4 = 4.7 \times 10^4$ J/m$^3$. We conclude that the epitaxial Fe(0 0 1) layer on the MgO(0 0 1) surface has higher structural quality compared with the case of Ag(0 0 1). This is because Ag grown on Pd(0 0 1) contains, along with preferred Ag(0 0 1), small amount of Ag(1 1 1) crystallites (Figure 2). These do not contribute to constant $K_4$ since there is no epitaxial growth of Fe(0 0 1) on the Ag(1 1 1) surface. The easy axes of the Fe/Ag(0.5 μm)/Pd sample also coincided with the [1 1 0] and [1 $\bar{1}$ 0] directions of the MgO(0 0 1) substrate. The orientation of the easy axes for all three samples corresponds to the epitaxial relationships (2).

Figures 4(b), 5(b), and 6(b) show the dependences of the fourfold anisotropy constant $K_4$ on the annealing temperature for the Pd/Fe, Fe/Ag(0.5 μm)/Pd, and Pd/Ag (1 μm)/Fe samples, respectively. With all samples, the values of $K_4$ remain invariable up to 400 °C, then drastically change after annealing at 450 °C. This fact confirms that the solid-state reaction is initiated between the Fe and Pd layers. For Pd/Fe, the fourfold in-plane anisotropy constant begins to sharply decrease after 400 °C and approaches

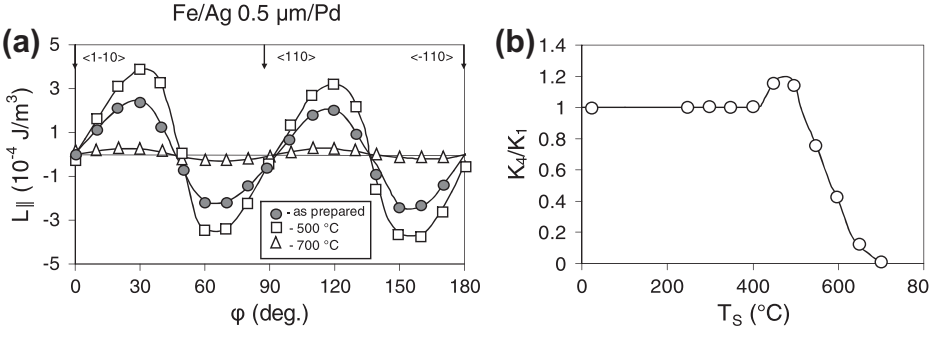


Figure 5. (a) Evolution of the in-plane fourfold torque curves $L\|(\varphi)$ (bulk Fe layer) for Fe/Ag(0.5 μm)/Pd as a result of the solid-state reaction between Pd with Fe via the inert Ag (0.5 μm) layer at different annealing temperatures $T_S$. The magnetocrystalline anisotropy constant $K_1 = 4.7 \times 10^4$ J/m$^3$ for the Fe (0 0 1) layer was determined from the torque curves for the as-deposited sample. (b) Relative in-plane fourfold magnetic constant $K_4/K_1$ for Pd/Ag (0.5 μm)/Fe as a function of annealing temperature $T_S$. The growth of the in-plane fourfold magnetic constant $K_4$ in the temperature range 450–500 °C is related to the formation of three types of crystallites of the magnetically hard $L1_0$-FePd phase [41]. The sharp drop of $K_4$ at 700 °C is related to the formation of the disordered magnetically soft $Fe_xPd_{1-x}$ phase [42].

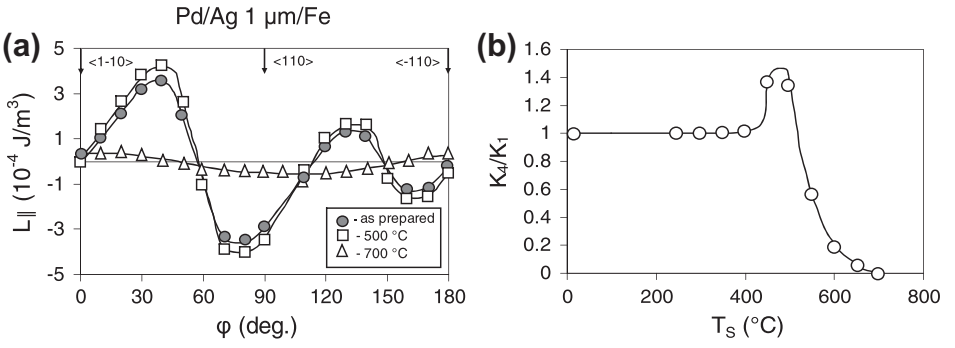


Figure 6. (a) Evolution of the in-plane fourfold torque curves $L\|(\varphi)$ (bulk Fe layer) for Pd/Ag (1 μm)/Fe as a result of the solid-state reaction between Pd and Fe via the inert Ag(1 μm) layer at different annealing temperatures $T_S$. The magnetocrystalline anisotropy constant $K_1 = 5.0 \times 10^4$ J/m$^3$ for the Fe (0 0 1) layer was determined from the torque curves for the as-deposited sample. (b) Relative in-plane fourfold magnetic constant $K_4/K_1$ for Pd/Ag(1 μm)/Fe as a function of annealing temperature $T_S$. The growth of the in-plane fourfold magnetic constant $K_4$ in the temperature range 450–500 °C is related to the formation of three types of crystallites of the magnetically hard $L1_0$-FePd phase [41]. The sharp drop of $K_4$ at 700 °C is caused by the formation of the disordered magnetically soft $Fe_xPd_{1-x}$ phase [42].

zero after annealing at 700 °C (Figure 2(b)). After annealing at 500 °C, the torque curves $L(\varphi)$ change the fourfold anisotropy to eightfold anisotropy atypical for the (0 0 1)$L1_0$ crystal plane (Figure 4(a)).

The magnetocrystalline anisotropy energy $E_K$ for the tetragonal crystal ($L1_0$ phase) per unit volume is [56]

$$E_K = E_0 + K_1 \cdot \sin^2\varphi + K_2 \cdot \sin^4\varphi + K_3 \cdot \cos^2\alpha \cos^2\beta + \ldots, \quad (4)$$

where $\varphi$ is the angle between the magnetization $M_S$ and the c axis [0 0 1], and $\alpha$ and $\beta$ are the angles between the magnetization $M_S$ and the [1 0 0] and [0 1 0] axes, respectively.

According to Equation (4), the torque curve in the (0 0 1)$L1_0$ crystal plane is described by the fourth-order curve $L(\varphi) = 1/2 \times K_3 \times \sin 4\varphi$. It was shown in [41], however that eightfold anisotropy is characteristic of the (0 0 1)$L1_0$-FePd. This is probably caused by the value $K_3 \sim 0$ for the $L1_0$-FePd phase; therefore, in expression (4) the higher order terms in the expansion of energy $E_K$ over the direction cosines should be taken into account. The dependences of the fourfold anisotropy constant $K_4$ on the annealing temperature for samples of Fe/Ag(0.5 μm)/Pd (Figure 5(b)) and Pd/Ag(1 μm)/Fe (Figure 6(b)) are identical. Unlike for the case of Pd/Fe (Figure 4(b)), above 400 °C the fourfold anisotropy constant starts growing and drops only after annealing at 500°C. According to the X-ray data, the highly anisotropic $L1_0$-FePd phase forms in this temperature range. The occurrence of the (2 0 0)$L1_0$-FePd reflection for samples of Fe/Ag (0.5 μm)/Pd (Figure 2) and Pd/Ag(1 μm)/Fe (Figure 3) suggests that the structure of the reaction product layer contains three types of $L1_0$-FePd crystallites, with three orthogonal axes parallel to the three main ⟨1 0 0⟩ axes of the MgO substrate.

Crystallites with the $c$ axes coinciding with the [1 0 0] and [0 1 0] MgO(0 0 1) directions, along with the relative volumes $f_1$ and $f_2$, induce the fourfold in-plane anisotropy with the constant $K_{4\ ||} = (f_1 + f_2)K_2$. This constant is determined by the second magnetocrystalline anisotropy constant $K_2 = (1.5 \pm 0.5) \times 10^5$ J/m$^3$ of the $L1_0$-FePd phase [41].

The results of magnetic measurements confirm a structural difference in the formation of $L1_0$-FePd between the Pd/Fe with the Fe/Ag(0.5 μm)/Pd and Pd/Ag(1 μm)/Fe samples. For the Fe/Ag(0.5 μm)/Pd and Pd/Ag(1 μm)/Fe samples, crystallites of the $L1_0$-FePd phase are arranged such that the $c$ axes are parallel to the ⟨1 0 0⟩ axes of the MgO substrate; the Pd/Fe samples only have the (0 0 1) orientation. Therefore, the contribution of $K_4$ || to the constant $K_4$ defines the increment $K_4/K_1$ in a temperature interval of 400–500 °C for samples of Fe/Ag(0.5 μm)/Pd (Figure 5(b)), and Pd/Ag (1 μm)/Fe (Figure 6(b)).

After annealing at 700 °C, only the uniaxial anisotropy remains in the plane of the Pd/Fe, Fe/Ag(0.5 μm)/Pd, and Pd/Ag(1 μm)/Fe samples. The absence of fourfold in-plane anisotropy indicates that the disordered fcc $Fe_xPd_{1-x}$ phase that is epitaxially grown at this temperature has a small first magnetocrystalline anisotropy constant $K_1$. This constant, estimated in the fcc $Fe_{50}Pd_{50}$ single crystals determined from the magnetization curves at 4.2 K, is $K_1 \sim 10^4$ J/m$^3$ [57]. Our results show that $K_1$ in fcc $Fe_{50}Pd_{50}$ at room temperature is negative and has an absolute value smaller than the measurement error of the torque method ($-1.0 \times 10^3$ J/m$^{3)}$. The exact value of the magnetic anisotropy constant of the disordered $FePd_3$ phase determined by the ferromagnetic resonance measurements is $K_1 = -2.0 \times 10^2$ J/m$^3$ [42].

Since magnetocrystalline anisotropy is a fundamental characteristic of a substance, any change in its constant results in structural changes in a sample. The variation in the constant $K_4$ above ~400 °C for all three types of samples confirms the X-ray data at the beginning of the solid-state reaction between Fe and Pd. The increment of $K_4/K_1$ for samples of Fe/Ag(0.5 μm)/Pd (Figure 5(b)) and Pd/Ag(1 μm)/Fe (Figure 6(b)) and the formation of the eightfold anisotropy in Pd/Fe (Figure 4(a)) in the temperature range 400–500 °C are related to the existence of the $L1_0$-FePd phase. The decrease in the absolute value of $K_4$ down to zero after annealing at 700 °C is consistent with the formation of the magnetically soft $Fe_xPd_{1-x}$ phase.

### 3.3. *Mössbauer study*

Figures 7–9 show (a) the Mössbauer spectra, and (b) the corresponding hyperfine magnetic field distributions P(H) for the Pd/Fe, Fe/Ag(0.5 μm)/Pd, and Pd/Ag(1 μm)/Fe samples, respectively, as-grown and annealed at temperatures up to 700 °C. All the as-grown samples contain the only phase with Mössbauer parameters close to those of the α-Fe phase. However, the hyperfine field $H = 320$ kOe appeared lower than 330 kOe for bulk α-Fe. This is probably caused by structural defects forming in the α-Fe layer during its epitaxial growth on MgO(0 0 1). As the annealing temperature increases to 400 °C, the structural quality of the α-Fe layer grows for all the samples, and the Mössbauer parameters approach those of bulk α-Fe. The ratio between the sextet line squares is close to 3:4:1:1:4:3; i.e. the magnetic moments of the iron atoms lie in the film plane. The absence of mixing of the layers in the as-grown Pd/Fe, Fe/Ag(0.5 μm)/Pd, and Pd/Ag(1 μm)/Pd samples up to an annealing temperature of 400 °C, as well as the absence of contributions from other phases to

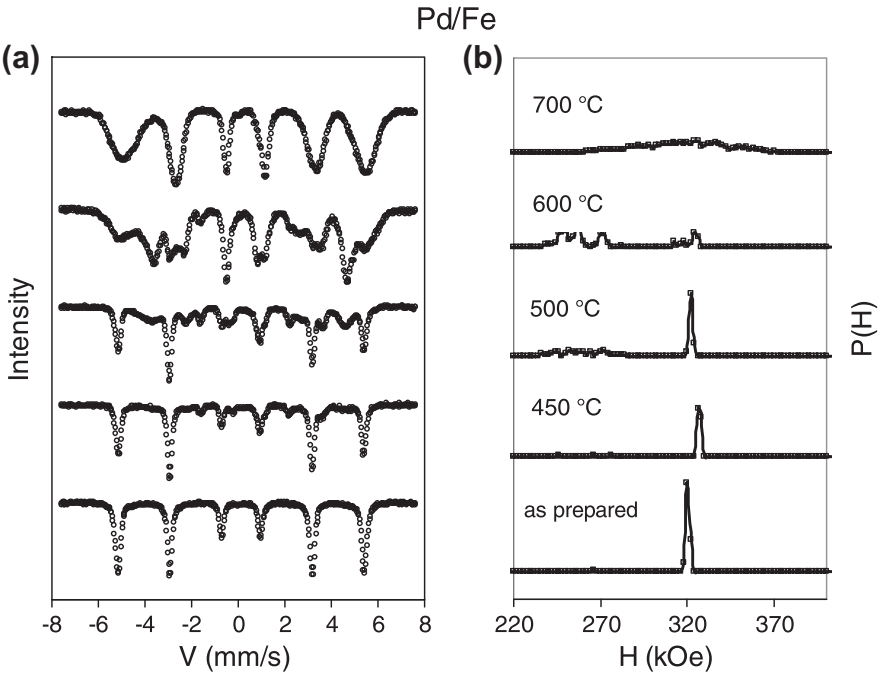


Figure 7. (a) Room-temperature $^{57}$Fe Mössbauer spectra, and (b) corresponding hyperfine distributions for the Pd/Fe film vs. annealing temperature $T_S$.

the Mössbauer spectra, is consistent with the X-ray data and anisotropy studies. The Mössbauer spectra of all the samples begin to change after annealing at 450 °C.

### 3.3.1. *Pd/Fe samples*

After annealing of the Pd/Fe bilayer at 450 °C, peaks at 200 and 260 kOe appear in the P(H) distribution in addition to the peak at 330 kOe corresponding to α-Fe (Figure 7(b)). This indicates the start of the effect of large mixing on the Pd/Fe interface and the formation of compounds. Approximating the general spectrum by three sextets and fitting the model spectrum to the experimental spectrum yield the Mössbauer parameters given in Table 1. The magnetic moments of 72% of the iron atoms in the α-Fe layer lie in the film plane; 11% of iron atoms have parameters IS = 0.22 mm/s, $H$ = 259 kOe, and QS = 0.17 mm/s. The Mössbauer parameters are close to those of the $L1_0$-FePd phase for bulk and film samples [58–62]. The large projection of the average magnetic moment onto the gamma radiation direction indicates that the moment of the $L1_0$-FePd phase is perpendicular to the film plane. This is consistent with X-ray data and magnetic measurements that show that the ordered $L1_0$-FePd(0 0 1) phase epitaxially grows such that the $c$ axis is normal to MgO(0 0 1). The parameters for 17% of the Fe atoms are IS = 0.19 mm/s, $H$ = 204 kOe, and QS = 0; these correspond to the $Fe_{21}Pd_{79}$ alloy close to the ordered $L1_2$-$FePd_3$ phase [61].

Table 1. Mössbauer parameters for the Pd/Fe film at different annealing temperatures $T_S$.

| | IS, mm/s ±0.005 | $H$, kG ±5 | QS, mm/s ±0.02 | $A$ ±0.03 | Position |
|---|---|---|---|---|---|
| As prepared | 0.008 | 320 | 0.01 | 1 | α-Fe |
| 450 °C | −0.002 | 327 | 0 | 0.72 | α-Fe |
| | 0.225 | 259 | 0.17 | 0.11 | $L1_0$ |
| | 0.188 | 204 | 0 | 0.17 | $L1_2$ |
| 500 °C | 0.005 | 322 | 0 | 0.42 | α-Fe |
| | 0.176 | 278 | 0 | 0.09 | $L1_0$ |
| | 0.189 | 261 | 0.22 | 0.11 | $L1_0$ |
| | 0.186 | 246 | 0.50 | 0.19 | $L1_0$ |
| | 0.183 | 202 | 0.05 | 0.19 | $L1_2$ |
| 600 °C | 0.163 | 339 | −0.25 | 0.18 | $Fe_{68}Pd_{32}$ |
| | 0.036 | 315 | −0.18 | 0.10 | α-Fe |
| | 0.206 | 309 | 0.11 | 0.11 | $Fe_{50}Pd_{50}$ |
| | 0.192 | 277 | 0.37 | 0.09 | $L1_0$ |
| | 0.200 | 260 | 0.60 | 0.15 | $L1_0$ |
| | 0.202 | 248 | 0.83 | 0.21 | $L1_0$ |
| | 0.192 | 201 | 0 | 0.16 | $Fe_{25}Pd_{75}$ |
| 700 °C | 0.178 | 318 | −0.09 | 1 | $Fe_{60}Pd4_0$ |

Note: Here IS is the isomer chemical shift relative to α-Fe; $H$ is the hyperfine magnetic field on Fe nuclei; QS is quadrupole splitting; $A$ is the relative spectral area.

After annealing at 500 °C, the α-Fe hyperfine field somewhat decreases due to the structural defects occurring when the $L1_0$-FePd phase is formed. The α-Fe fraction drops to 41%. The $L1_0$-FePd phase is found to be inhomogeneous in the local characteristics of iron positions. Three iron positions are identified to be different in the hyperfine fields (278, 261, and 246 kOe), quadrupole splittings (0, 0.22, and 0.50 mm/s), and fractions (9, 10, and 18%) (see Figure 7(b) and Table 1). The spread of the Mössbauer parameters for the $L1_0$-FePd phase is probably caused by the features of the disordering $L1_0 \rightarrow A_1$ that start above 500 °C. The population and characteristics of the $L1_2$-$FePd_3$ phase remain invariable.

After annealing at 600 °C, the α-Fe fraction drops to 10%. The small hyperfine field (315 kOe), large quadrupole splitting (−0.18 mm/s), and large chemical shift (0.036 mm/s) indicate the presence of structural defects in the α-Fe phase. The observed iron-rich disordered $Fe_{1-x}Pd_x$ alloys with hyperfine fields of 339 and 309 kOe correspond to compositions of about $Fe_{68}Pd_{32}$ and $Fe_{50}Pd_{50}$, respectively. The phase with a characteristic hyperfine field of 200 kOe is $Fe_{25}Pd_{75}$, formed due to the disordering of the $L1_2$-$FePd_3$ phase.

After annealing at 700 °C, a wide distribution of hyperfine fields (250–370 kOe) is observed. This is related to the formation of disordered $Fe_xPd_{1-x}$ phases over a wide composition range (Figure 7(b)). Approximating the spectrum by one sextet yields average parameters characteristic of the disordered phase of the $Fe_{60}Pd_{40}$ composition.

### 3.3.2. *Fe/Ag(0.5 μm)/Pd sample*

After annealing at 450 °C, the Mössbauer spectrum of the Fe/Ag(0.5 μm)/Pd sample contains the α-Fe phase (74%), with the magnetic moments of iron atoms lying in the film plane (Figure 8).

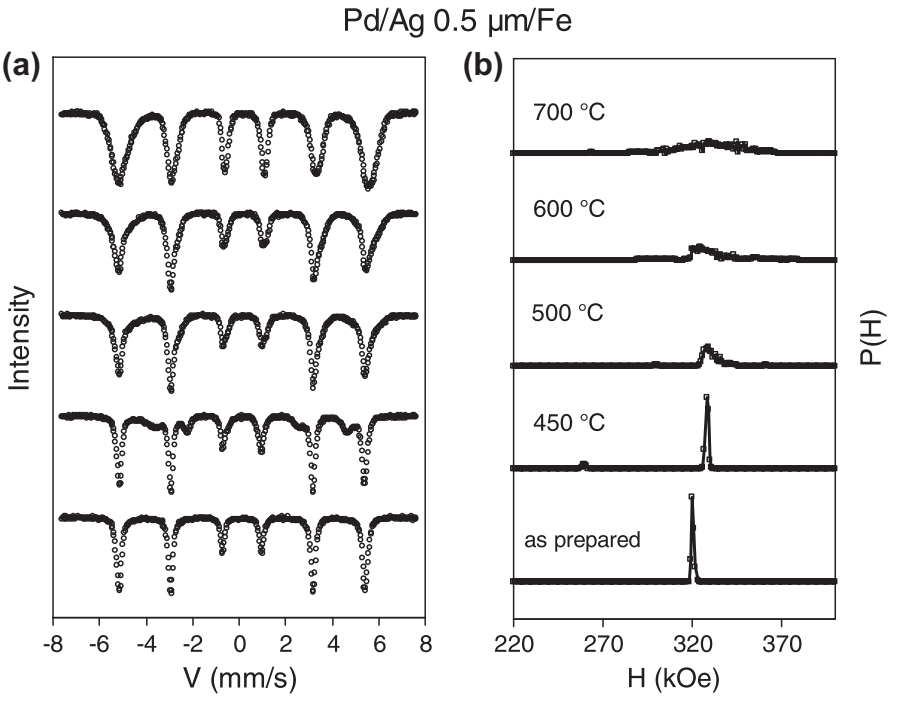


Figure 8. (a) Room-temperature $^{57}$Fe Mössbauer spectra, and (b) corresponding hyperfine distributions for the Pd/Ag(0.5 μm)/Fe film vs. annealing temperature $T_S$.

Table 2. Mössbauer parameters for the Pd/Ag(0.5 μm)/Fe film at different annealing temperatures $T_S$.

| | IS, mm/s ±0.005 | $H$, kOe ±5 | QS, mm/s ±0.02 | $A$ ±0.03 | Position |
|---|---|---|---|---|---|
| As prepared | 0.008 | 320 | 0.01 | 1 | α-Fe |
| 450 °C | 0 | 328 | 0 | 0.74 | α-Fe |
| | 0.206 | 260 | 0.63 | 0.26 | $L1_0$ |
| 500 °C | 0.167 | 345 | −0.26 | 0.29 | $Fe_{75}Pd_{25}$ |
| | 0 | 330 | 0 | 0.55 | α-Fe |
| | 0.305 | 320 | 0.07 | 0.10 | $Fe_{50}Pd_{50}$ |
| | 0.187 | 287 | 0.29 | 0.06 | $L1_0$ |
| 600 °C | 0.152 | 349 | −0.10 | 0.15 | $Fe_{75}Pd_{25}$ |
| | 0.182 | 332 | −0.23 | 0.27 | $Fe_{60}Pd_{40}$ |
| | 0.014 | 326 | −0.01 | 0.49 | $Fe_{55}Pd_{45}$ |
| | 0.307 | 317 | 0.24 | 0.09 | $Fe_{50}Pd_{50}$ |
| 700 °C | 0.108 | 331 | −0.02 | 1 | $Fe_{60}Pd_{40}$ |

The other component (26%) is the $L1_0$-FePd phase, in which the magnetic moments of the iron atoms have no preferred direction (Table 2). This is consistent with X-ray data and magnetic measurements that show three types of crystallites of the ordered

$L1_0$ phase, growing such that the *c* axes are parallel to the three main ⟨1 0 0⟩ axes of the MgO substrate.

After annealing at 500 °C, the solid-state reaction between Fe and Pd continues, and as a result, the α-Fe and $L1_0$-FePd fractions drop to 55 and 6%, respectively (Table 2). The $L1_0$-FePd phase transforms to the disordered $Fe_{50}Pd_{50}$ phase, and disordered high-iron alloys are formed that have an approximate composition $Fe_{75}Pd_{25}$ (29%) (Table 2).

Annealing at 600 °C leads to further dilution of the Fe layer and the disappearance of positions that have parameters typical of α-Fe. The iron positions with Mössbauer parameters characteristic of disordered $Fe_{1-x}Pd_x$ alloys arise; the Fe content in these positions is 50–75% (Table 2).

After annealing at 700 °C, the Mössbauer spectrum becomes typical of an amorphous substance (Figure 8(a)). Similar to that of the Pd/Fe sample, the hyperfine field distribution is wide, between 300 and 370 kOe (Figure 6(b)). The one-sextet approximation of the spectrum yields average parameters that are characteristic of the disordered layer of an approximate composition $Fe_{60}Pd_{40}$ (Table 2).

### 3.3.3. *Pd/Ag(1 μm)/Fe sample*

After annealing at 450 °C, the Mössbauer spectrum of the Pd/Ag(1 μm)/Fe sample (Figure 9) and the parameters of its hyperfine structure (Table 3) show only the contribution of α-Fe.

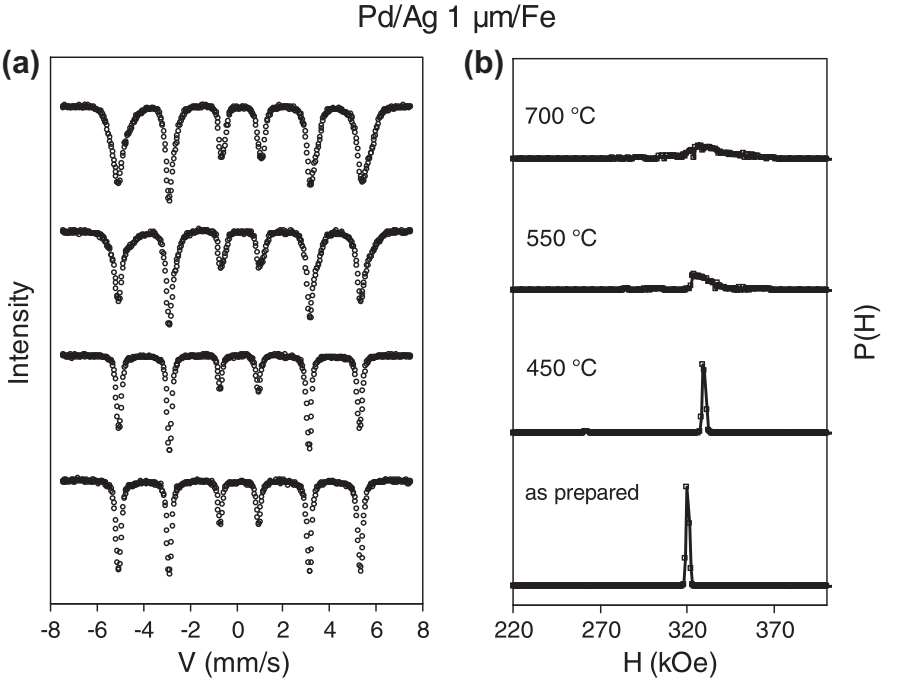


Figure 9. (a) Room-temperature $^{57}$Fe Mössbauer spectra, and (b) corresponding hyperfine distributions for the Pd/Ag(1 μm)/Fe film vs. annealing temperature $T_S$.

Table 3. Mössbauer parameters for the Pd/Ag(1 μm)/Fe film at different annealing temperatures $T_S$.

| | IS, mm/s ±0.005 | $H$, kOe ±5 | QS, mm/s ±0.02 | $A$ ±0.03 | Position |
|---|---|---|---|---|---|
| As prepared | 0.008 | 320 | 0.01 | 1 | α-Fe |
| 450 | −0.007 | 330 | 0.01 | 1 | α-Fe |
| 550 °C | 0.134 | 349 | −0.08 | 0.26 | $Fe_{75}Pd_{25}$ |
| | 0.031 | 329 | 0 | 0.62 | α-Fe |
| | 0.181 | 308 | 0.15 | 0.12 | $Fe_{50}Pd_{50}$ |
| 700 | 0.065 | 333 | 0.03 | 1 | $Fe_{70}Pd_{30}$ |

After annealing at 550 °C, the fraction of the α-Fe layer decreases to 62% and the disordered phases of approximate compositions $Fe_{75}Pd_{25}$ and $Fe_{50}Pd_{50}$ begin to form (Table 3). This is caused by mixing of the Fe and Pd layers, which is not inhibited even by the Ag(1 μm) buffer layer. After annealing at 500 °C, the Mössbauer spectrum (Figure 9) does not show the component of the $L1_0$-FePd phase, although according to X-ray and magnetic studies, this phase occurs in the Pd/Ag(1 μm)/Fe sample at this temperature. Perhaps, this is because the amount of the $L1_0$-FePd phase is small (below 5%). The disordered phase of a $Fe_{50}Pd_{50}$ composition forms, likely due to disordering of the $L1_0$-FePd phase.

After annealing at 700 °C, the Mössbauer spectrum shows no α-Fe contribution; instead, a continuous series of disordered $Fe_xPd_{1-x}$ solid solutions forms. The hyperfine field distribution has a broad peak within 280–360 kOe (Figure 9(b)) with the maximum about 333 kOe. According to [58], this corresponds to a disordered phase of approximate composition $Fe_{70}Pd_{30}$ (Table 3).

Thus, the data from the Mössbauer study are consistent with the results of the X-ray investigations and magnetic measurements, showing that solid-state reactions in samples of Pd/Fe, Fe/Ag(0.5 μm)/Pd, and Pd/Ag(1 μm)/Fe begin above 400°C. The data also confirm the successive formation of the $L1_0$-FePd and disordered $Fe_xPd_{1-x}$ phases with an increase in the annealing temperature to 700°C.

### 3.4. *XPS study*

We performed XPS measurements of the surface chemical composition at different annealing temperatures to clarify the features of atomic migration during the thin-film solid-state reaction between Pd and Fe in the Fe/Ag(0.5 μm)/Pd and Pd/Ag(1 μm)/Fe samples. After annealing, the sample's surface is noticeably oxidized; however, $Ar^+$ ion sputtering of the surface layer with a thickness of 2–5 nm completely removes the carbon and reduces the oxygen concentration to 10–15%. In the Fe/Ag(0.5 μm)/Pd sample, the contribution of the oxide component to the Fe 2p spectra significantly decreases and Fe(0) (pure metallic Fe) becomes the main component. Since no iron oxides or carbides are observed in the Mössbauer spectra, we conclude that the upper layer consists mainly of Fe(0).

#### 3.4.1. *Evolution of the surface composition in the Fe/Ag(0.5 μm)/Pd sample*

It is seen in Figure 10 that in the Fe/Ag(0.5 μm)/Pd samples, beginning from an annealing temperature of 400 °C, the relative concentration of iron decreases and that of

palladium increases. The Ag signal also appears; however, the Ag concentration on the surface remains insignificant. Figure 11 shows that for the Fe/Ag(0.5 μm)/Pd samples, the binding energies of the Pd $3d_{5/2}$ peak increase after annealing at temperatures above 400 °C, and the displacement attains 0.85 eV at 700 °C.

The occurrence of the signal from palladium and the change in its binding energy can be explained by the formation of $Fe_xPd_{1-x}$ alloys due to the migration of Pd atoms via the inert Ag layer to the top Fe layer, as well as the structural rearrangement Fe/Ag (0.5 μm)/Pd → $Fe_xPd_{1-x}$/Ag(0.5 μm). As was previously shown for $Fe_xPd_{1-x}$ alloys, as the iron concentration increases, the Fe 2p line shifts to lower binding energies and the Pd 3d line shifts to higher binding energies [62,63]. The iron concentration in $Fe_xPd_{1-x}$ is related to the binding energy as $x = \Delta E/1.6$ [62]. Substituting the value $\Delta E = 0.85$ эВ, we obtain the alloy composition $Fe_{53}Pd_{47}$; however, the composition determined from the photoelectron line intensity is $Fe_{65}Pd_{35}$ at an annealing temperature of 700 °C. These data are consistent with the results of the Mössbauer and X-ray studies indicating the formation of the ordered $Ll_0$-FePd phase of the equiatomic composition at 500 °C, and of the iron-rich disordered $Fe_xPd_{1-x}$ alloys ($x \sim 60$–70%) above 600 °C. We therefore believe that the more exact composition for 700 °C is $Fe_{65}Pd_{35}$.

### 3.4.2. *Evolution of the surface composition in the Pd/Ag(1 μm)/Fe sample*

The photoelectron spectra of the Pd/Ag(1 μm)/Fe/MgO sample also change starting from 400 °C, but in a different way (Figure 12). The Fe line intensity is nearly invariable and very low. This means that there is small amount of Fe on the surface, with no noticeable migration of Fe atoms via the Ag barrier and the top palladium layer to the sample's surface. At the same time, after annealing at 400 °C, the Pd 3d peak intensity decreases and the Ag 3d peak intensity sharply increases. One can see visually that there is no Pd on the sample's surface after annealing at temperatures above 550 °C. The surface of the as-grown Pd/Ag(1 μm)/Fe sample changes the dark-grey colour of

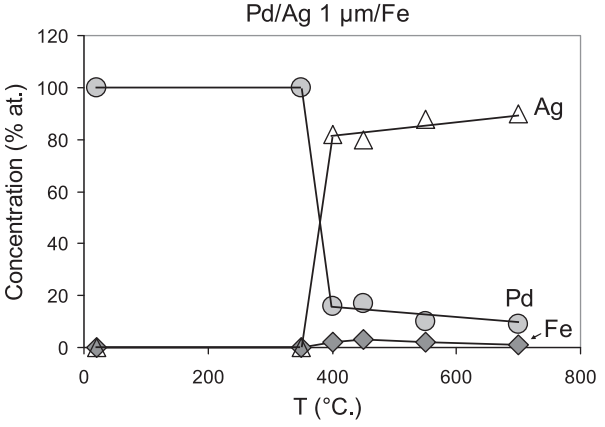


Figure 10. Atomic concentrations of Fe(♦), Pd(●), and Ag(Δ) vs. annealing temperature $T_S$ for the Fe/Ag(0.5 μm)/Pd sample. After annealing at 700 °C, the $Fe_{67}Pd_{33}$ surface alloy forms as a result of the migration of Pd to the top Fe layer via the inert Ag(0.5 μm) barrier.

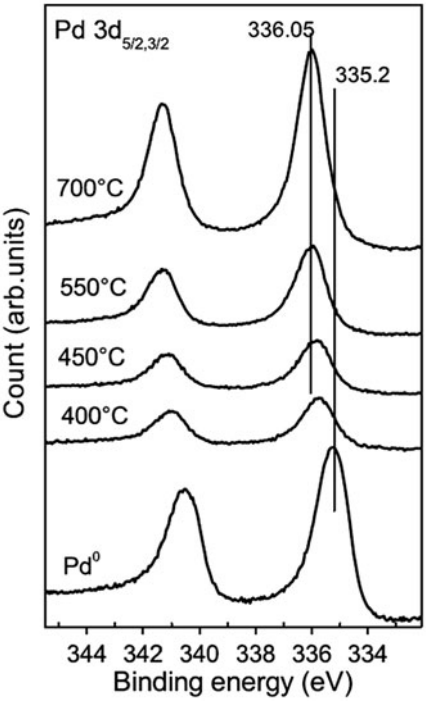


Figure 11. Pd 3d XPS spectra of the $Fe_xPd_{1-x}$ film grown in the reaction between Fe and Pd on the Fe/Ag(0.5 μm)/Pd sample after annealing at 400, 450, 550, and 700 °C. The vertical lines mark the positions of the Pd $3d_{5/2}$ photoelectronic lines for bulk Pd 3d and the $Fe_xPd_{1-x}$ alloys.

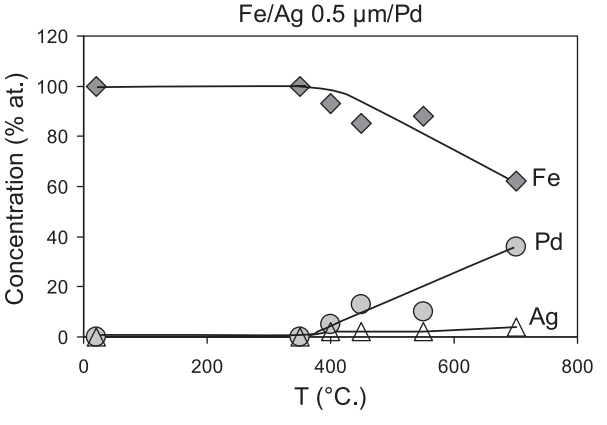


Figure 12. Atomic concentrations of Fe(♦), Pd(●), and Ag(Δ) vs. annealing temperature $T_S$ for the Pd/Ag(1 μm)/Fe sample. After annealing at 700 °C, the top Pd layer almost completely vanishes from the surface of the Pd/Ag(1 μm)/Fe sample. Analysis of XRD, Mössbauer spectroscopy, and magnetic data shows the migration of Pd to the lower Fe layer via the inert Ag(1 μm) barrier.

the Pd film to a mirror image of the Ag layer. These changes can be caused by adsorption of Pd from the Ag surface and/or migration of Pd to the inert Ag barrier. Along with the magnetic, Mössbauer, and X-ray measurements, these results indicate the preferred migration of Pd atoms via the inert Ag barrier for the solid-state reaction between Pd and Fe. This means that Pd is the dominant moving species in the successive formation of the $L1_0$ phase and the disordered $Fe_xPd_{1-x}$ alloy. In other words, after annealing at 700 °C, the solid-state reaction leads to the structural transformation Pd/Ag (1 μm)/Fe → Ag(1 μm)/$Fe_xPd_{1-x}$. The dominant moving species in thin-film solid-state reactions have been determined in a number of studies [23–26]. It was shown, in particular, that Pd atoms are the dominant moving species in the formation of $Pd_2Si$ [23].

Assuming that the forming $Fe_xPd_{1-x}$ alloy is homogeneous over its volume for both Pd/Ag(1 μm)/Fe and Fe/Ag(0.5 μm)/Pd, and knowing its concentration, we can calculate the fraction of the initial Pd layer migrated to the Fe layer with a thickness of 180 nm. After annealing at 700 °C, the alloy composition is $Fe_{65}Pd_{35}$, i.e. 115 nm of the initial 130 nm of the Pd layer participated in the formation of the alloy. It would be impossible if atoms transferred only by diffusion, because in this case a considerable proportion of the Pd atoms should remain in the initial layer or stick in the Ag barrier.

## 4. Discussion

### 4.1. *Comparison of XRD, magnetic anisotropy, Mössbauer spectroscopy, and XPS data*

Figure 13 summarizes the phase transformations occurring in samples of Pd/Fe, Fe/Ag (0.5 μm)/Pd, and Pd/Ag(1 μm)/Fe with increasing annealing temperature, as revealed by X-ray, magnetic anisotropy, Mössbauer spectroscopy, and XPS studies. For all samples, regardless of the thickness of the inert Ag layer, the reaction between Pd and Fe begins at temperatures above 400 °C with the formation of the first $L1_0$-FePd phase. For Pd/Fe, the ordered $L1_2$-$FePd_3$ phase also forms above 400 °C. This implies similar initiation temperatures for the $L1_0$-FePd and $L1_2$-$FePd_3$ phases. However, no $L1_2$-$FePd_3$ phase is observed in the Fe/Ag(0.5 μm)/Pd and Pd/Ag(1 μm)/Fe samples at any annealing temperature. As the annealing temperature is increased above 500 °C, the disordered $Fe_xPd_{1-x}$ phase arises in all samples and dominates after 700 °C. Palladium atoms become the dominant moving species in the solid-state reactions in the Fe/Ag(0.5 μm)/Pd and Fe/Ag(0.5 μm)/Pd samples. It should be noted that the migration of Pd atoms in Fe(0 0 1) does not break the epitaxial Ag(0 0 1) barrier layer even at a thickness of 1 μm. This indicates that the atomic transport, without significant embedding in a grain, moves along the grain boundaries, dislocations, or pinholes which frequently form during solid-state reactions [64,65]. Regardless of the Ag buffer layer thickness, embedding Pd atoms in the epitaxial Fe(0 0 1) layer leads to the successive epitaxial growth of the ordered $L1_0$-FePd (0 0 1) and $L1_2$-$FePd_3$(0 0 1) and the disordered $Fe_xPd_{1-x}$(0 0 1) phases.

### 4.2. *The LRCI effect in thin-film solid-state reactions*

According to the phase equilibrium diagrams, Ag does not mix with either Fe or Pd up to 960 °C. The experimental data reported above confirms an absence of mixing on the

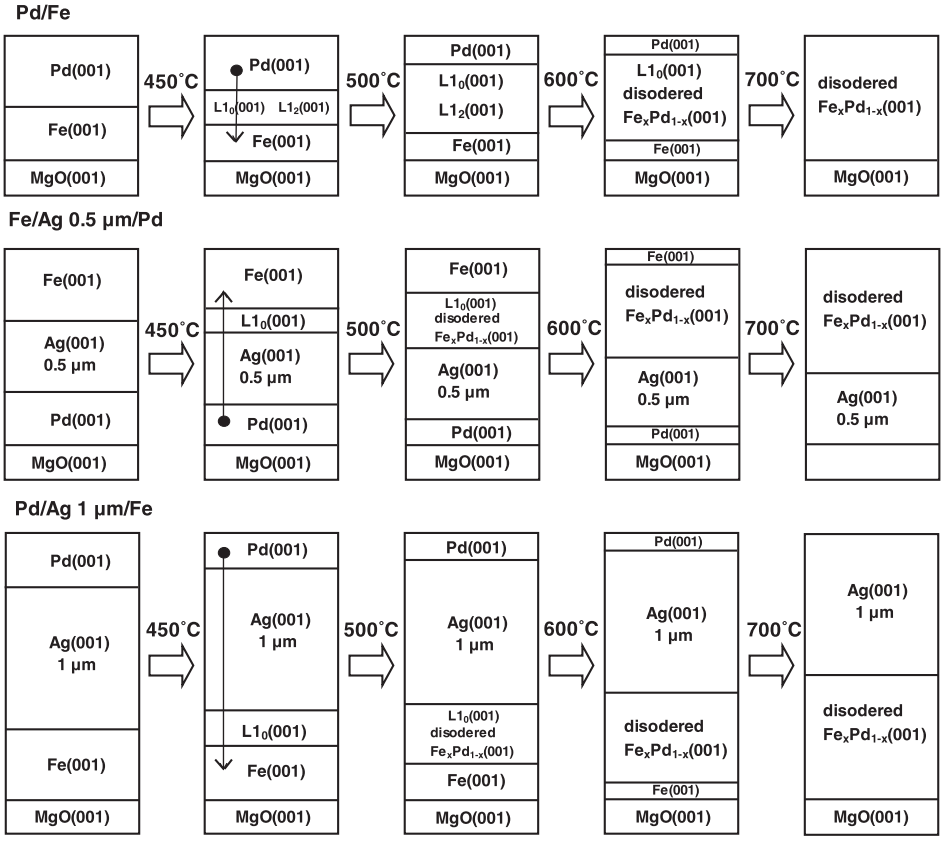


Figure 13. Schematic diagram showing the absence of the effect of the inert Ag (0 0 1) buffer layer placed between the reacting Fe(0 0 1) and Pd(0 0 1) films on the synthesis of the $L1_0$-FePd (0 0 1), $L1_2$-$FePd_3$(0 0 1), and $Fe_xPd_{1-x}$(0 0 1) phases. The arrow points the dominant migration of Pd atoms to the Fe layer during the solid-state reaction between Fe and Pd. Regardless of the thickness of the inert Ag (0 0 1) buffer layer, the reaction between Pd and Fe starts at 450 °C with the formation of the ordered $L1_0$-FePd phase and finishes at 700 °C with the formation of the disordered $Fe_xPd_{1-x}$ phase.

Ag/Pd and Ag/Fe interfaces up to 700 °C. This is consistent with data at the start of significant interdiffusion of Ag and Fe atoms on the Ag/Fe(0 0 1) interface, only above 900 °C [66,67]. Furthermore, the surface alloy on the interface in Ag/Pd(1 1 1) is stable in the temperature range 250–500 °C, and the pure Pd(1 1 1) surface recovers at high annealing temperatures (up to ~930 °C) [68]. A combination of XRD and energy dispersive X-ray analyses reveals that co-deposited Pd and Ag are in separate phases [69].

The absence of diffusion in the Ag/Pd and Ag/Fe bilayers up to 700 °C, as well as the fast migration of Pd via the inert Ag layer with the formation of $L1_0$-FePd in the Fe/Ag(0.5 μm)/Pd and Pd/Ag(1 μm)/Fe trilayers above 400 °C clearly demonstrate that during the solid-state reaction, a moving force of atomic migration is not diffusion. This leads us to suggest a new mechanism for atomic transport via a diffusion barrier or a

reaction product layer during solid-state reactions. The moving force of atomic migration is not a random diffusion walk, but instead is a strong chemical interaction between Fe and Pd atoms via the inert Ag layer that results in the synthesis of the $L1_0$-FePd phase. In the reacting state (above the initiation temperature), a strong chemical interaction between Pd and Fe atoms occurs that cannot be suppressed by the inert Ag buffer layer.

This proposed a sequential scenario of fast Pd atomic migration via an inert Ag(0 0 1) layer and synthesis of $L1_0$-FePd. Below 400 °C, Fe and Pd are chemically inert atoms. Above 400 °C, strong chemical interactions arise between Fe and Pd. Under these interactions, chemical bonds in the Pd layer break and the Pd atoms directionally migrate via the inert Ag(0 0 1) barrier to the Fe layer to initiate the synthesis of $L1_0$-FePd. The Pd propagates through the interior of the Ag(0 0 1) grain boundaries, dislocations and others structural defects or pinholes which frequently form during solid-state reactions [64,65]. Since the Fe and Pd atoms do not chemically interact with the Ag atoms, it is reasonable to suggest that the chemical interaction between Fe and Pd atoms works at a distance over 1 μm. In other words, the radius of this chemical interaction exceeds the ordinary chemical bond length in metals by a factor of $\sim 10^4$.

The effect of LRCIs in the thin-film solid-state reactions is experimentally confirmed in the following thin-film systems.

(1) Fe/Ag/Ni

The solid-state reaction between Fe and Ni atoms begins at a temperature of 350 °C, which coincides with the temperature of the eutectoid decomposition in the Fe–Ni system [66,67,70]. However, a 0.9 μm-thick inert silver layer placed between the Fe and Ni films does not suppress the reaction between the Fe and Ni atoms, and only somewhat increases the initiation temperature [66].

(2) Au/Co/Cu

Previous investigations showed that interdiffusion in bimetallic Au/Cu films already occurs at a low temperature (160–220 °C) with the formation of the $CuAu_3$ and $Cu_3Au$ phases [71,72]. Madakson [73–75] observed interdiffusion of Au and Cu at 250 °C in Au/Cu bilayers and at 450 °C in Au/Co/Cu trilayers with the formation of CuAu, $Cu_3Au$, and $Cu_3Au_2$ compounds. Furthermore, this author demonstrated for the first time that the chemically inert Co layer with a thickness up to 320 nm does not change the formation of the CuAu, $Cu_3Au$, and $Cu_3Au_2$ phases but only increases their initiation temperatures. An analysis of these data shows that interdiffusion Cu and Au are consequent to the formation of intermetallic Cu–Au compounds.

In an earlier work [76], we reported thin-film solid-state reactions in Au/Cu bilayers and showed that at heating rates above 20 K/s in these bilayers deposited on glass substrates, the reaction occurs in an autowave mode (combustion wave). In epitaxial Au/Cu(0 0 1)/MgO(0 0 1), the reaction between Au and Cu leads to the formation of epitaxial CuAu I, CuAu II, and $Cu_3Au$ ordered phases [76]. Within experimental error, the temperature of the start of the reaction coincides with the minimum temperature (240 °C) of the order–disorder transition in the Cu–Au system [77].

The reaction is not suppressed if an epitaxial layer of cubic Co(0 0 1) with thicknesses of 210 and 480 nm is deposited between Au and Cu(0 0 1). An unprecedented

result is obtained on a Au/Co(0 0 1)/Cu(0 0 1) trilayer system where Au and Cu atoms react via an inert Co(0 0 1) layer with a thickness of 2.5 μm [78]. This suggests fast atomic transport and a large effective diffusivity of the reacting Au and Cu atoms in Co (over $10^{-15}$ $m^2/s$).

(3) Au/Fe/Cd

As shown previously, the solid-state synthesis of martensitic phases in Cd/Au bilayers starts at the temperature of martensitic transformation (67 °C) in the Au–Cd system [79,80]. However, spatially separating the Cd and Au films using a 0.42 μm-thick inert epitaxial Fe(1 1 0) layer does not suppress the reaction in the Cd/Fe(1 1 0)/Au(1 1 1) film systems [81]. The reaction also occurs upon deposition of Cd onto polycrystalline Fe/Au films above the martensitic transformation temperature. The photoelectron study shows that Cd is the dominant moving species in the Cd/Fe thin-film reaction [81].

(4) Cu/Fe/β-CuZn

The diffusion of Cu in beta brass was investigated in classic Kirkendall experiments. After long-term annealing, the interdiffusion of Cu and Zn initiated a solid-state reaction in which an α-CuZn layer grew and reduced the thickness of an initial β-CuZn layer. This effect was interpreted as direct experimental proof of the vacancy diffusion mechanism instead of the direct atomic exchange suggested earlier. The current explanation of the Kirkendall effect is based on a primary diffusion of Zn from β-CuZn to the Cu layer and a secondary synthesis of α-CuZn [82–84]. Myagkov et al.[85] studied the reaction between Cu and the β-CuZn layer via inert Fe barrier layers with a thickness up to 0.85 μm in Cu/Fe/β-CuZn film systems. It was shown that Zn is the dominant diffusing species. The formation of α-CuZn regardless of the Fe barrier thickness strongly suggests that with the Kirkendall effect, the moving force of migration of Zn atoms from β-CuZn to the Cu layer is the strong LRCI between Zn and Cu atoms, and is not diffusion flow caused by a concentration gradient, as was generally agreed.

The literature review shows that long-range atomic transfer via inert buffer layers has also been observed for the mass transport of Au and Pb atoms through an Ag(300 nm) interlayer [86], outdiffusion of Au through Pt(1 μm) [87], outdiffusion of Si through Au(230 nm) [88], and diffusion of Fe, Ni, and Co through an Au(300 nm) film [89].

To determine the maximum length of the chemical interaction, we investigated the solid-state reaction of the epitaxial Fe(0 0 1) layer with a polycrystalline Pd film via the Ag barrier with a thickness of 2.2 μm in Pd/Ag(2.2 μm)/Fe samples (these results are not presented here). X-ray diffraction and anisotropy studies clearly demonstrate that the Ag(2.2 μm) layer does not suppress Pd migration in the Fe layer. Weak reflections from $L1_0$-FePd and a strong Fe(2 0 0) peak occur after annealing at 550 °C; these phenomena show that only a minor portion of the Pd atoms migrates via the Ag(2.2 μm) barrier, reaches the Fe layer, and participates in the formation of the $L1_0$-FePd phase. After annealing at 650 °C, X-ray diffraction patterns contain a weak reflection from the disordered $Fe_xPd_{1-x}$(0 0 2) phase. This formation of the $Fe_xPd_{1-x}$(0 0 2) phase decreases the fourfold in-plane anisotropy constant $K_4$. As follows from the analysis of the migration of Pd atoms via thick Ag barriers, the maximum length of the chemical interaction between Pd and Fe at temperatures up to 700 °C is more than 2.2 μm.

For the Pd/Ag(2.2 μm)/Fe sample, the effective Pd diffusivity in Ag during the reaction is estimated by the Einstein formula to be $D_{\text{reaction}} \sim d^2/t = 10^{-14}\ \text{m}^2/\text{s}$. This value exceeds the interdiffusivity $D_{\text{diffusion}} \sim 7 \times 10^{-21}\ \text{m}^2/\text{s}$ in epitaxial thin films of Ag(1 1 1)–Pd(1 1 1) annealed at 500 °C by more than six orders of magnitude [90]. $D_{\text{reaction}}$ is consistent with interdiffusivity values in metal–metal and metal–Si multilayers [9]. The inequality $D_{\text{reaction}} \gg D_{\text{diffusion}}$ confirms the key role of chemical interactions in the atomic migration during thin-film solid-state reactions. The micrometer radius of the interaction ensures the large effective touch area of reacting particles and leads to their fast approach with the formation of a chemical bond. As soon as the reaction product layer exceeds the chemical interaction radius, it begins to grow further via very slow diffusion processes.

It has been shown that the initiation temperature $T_0$ of the solid-state reaction in bilayers and multilayers coincides with the minimum temperature of the structural solid-state transformation in the system [76,91–95]. In particular, the solid-state reaction between Au and Cu starts at the minimum temperature of the order–disorder transition (240 °C) in the Au–Cu system, with the formation of CuAuI and CuAuII superstructures [76]. The solid-state reactions in Co/Pt [91], Se/Cu [92], Ni/Fe, Cu/Fe [93,94], and Al/Ni [95] begin at the temperatures of the order–disorder transition, superionic transition, eutectoid decomposition, and reverse martensitic transition, which have the minimum temperature of structural phase transformations in Co–Pt, Se–Cu, Ni–Fe, Cu–Fe, and Al–Ni systems, respectively. We can therefore expect that low-temperature reactions occur only in bilayers and multilayers in which the reagents have a phase equilibrium diagram with low-temperature structural transformations.

Similar to the temperatures of solid-state transformations, the initiation temperatures of the first phase and phase sequence are universal characteristics of a reacting pair. They do not depend on the deposition method and morphology of film reagents, and they weakly depend on interface contamination. In our recent study [42], we suggested that the temperatures 400 and 450 °C at which the $L1_0$-FePd and $L1_2$-$FePd_3$ phases begin to form in Pd/Fe bilayers are the phase transition temperatures of these phases. The coincidence of the initiation temperatures $T_0$ with the structural transformation temperatures $T_K$ leads us to consider common mechanisms controlling the reactions and transformations in solids. In particular, the LRCIs should participate in solid-state transformations during the formation of long-period superstructures, eutectoid transformations, and spinodal decomposition.

The long-range effects are sufficiently studied and widely discussed in various fields of solid-state chemistry and the physics of condensed matter. These effects primarily include, for example, oriented growth through an amorphous buffer layer [96], the long-range effect of ionic implantation on the structure and properties of semiconductors and metals [97,98], long-range capillary interactions in liquid films [99], long-range atomic interactions in the melting of metal surfaces [100] and the long-range interaction between adsorbates on metal surfaces [101,102]. Recent advances in the theory, computation, and measurement of the long-range interactions in nanoscale science were reviewed in [103]. A novel direction in atomic physics is the experimental and theoretical study of the formation of purely long-range ultracold molecules by photoassociation (e.g. [104]). Giant helium dimers with the internuclear distances 1150 $\alpha_0$ ($\alpha_0 \approx 0.053$ nm is the Bohr radius) have been obtained [105]. A review [106] emphasizes the

importance of the long-range interactions in the theoretical description of chemical reactions at cold and ultracold temperatures.

The above arguments demonstrate that there is incomplete knowledge not only about atomic migration processes but also about the mechanisms of chemical interactions in solids. The occurrence of long-range interactions in different science fields supports that some of them are LRCIs.

### 4.3. *LRCIs and chemical bonds*

It is well known that all fundamental interactions in solids are described by short-range potentials. However, the nature of the chemical bonds which underlie these interactions remains a subject for discussion [107–111]. We believe that the chemical interaction between reacting atoms is not limited by a chemical bond length. The LRCI between reacting atoms is a fundamental characteristic of the initial stage of chemical reactions that precede the formation of a stable chemical bond.

At present, long-range intermolecular and interatomic interactions are often attributed to long-range attractive dispersion forces of electrodynamic origin, as they arise from the zero-point fluctuations of an electromagnetic vacuum [112–119]. In the nanoscale, these forces are van der Waals forces and for macroscopic bodies, they are known as Casimir forces. At distances about or larger than the characteristic absorption wavelength, the dispersion forces between atoms and between an atom and a wall are usually called Casimir–Polder forces. Although measurement of the dispersion forces is a challenging experimental problem, recent investigations using precise techniques have demonstrated that the Casimir forces for different geometries are measurable at distances from 0.1 to 3.0 μm [112–115], and the Casimir–Polder forces are measurable from 0.1 μm to over 7.0 μm [116–119]. The distances at which the dispersion forces work coincide with the radii of the chemical interactions during the solid-state reaction between Pd and Fe. Thus, we can suggest a common nature to these interactions. However, there are serious arguments against this suggestion. The dispersion forces are weak and rapidly decrease with increasing distance between macroscopic bodies. On the contrary, strong LRCIs can break chemical bonds on the microscale and they weakly depend on the distance between reacting layers.

Although the LRCIs originate from the study of solid-state reactions, they undoubtedly underlie any chemical reaction. We believe that the LRCIs broaden one's outlook regarding the nature of the chemical bonds and demonstrate that the notion of the chemical bond is many-sided and more completed than what is typically presented in science. The discovered feature of a chemical bond – the long-range character of chemical interactions – should underlie the formation of supramolecular structures, self-assembly mechanisms, self-organization phenomena, and the construction of a great number of biological objects.

## 5. Conclusions

We investigated the effect of a chemically inert Ag buffer layer on the solid-state reaction between epitaxial Pd(0 0 1) and Fe(0 0 1) films. To suppress the reaction, we chose two thicknesses of the chemically inert Ag film: 0.5 and 1 μm. For comparison, we used samples without a buffer layer in the experiments. At an annealing temperature

of 400 °C, in all samples the ordered $L1_0$-FePd(0 0 1) phase was the first to form. Regardless of the buffer layer thickness, above 500 °C the disordered $Fe_xPd_{1-x}$(0 0 1) phase begins to form and becomes the only phase at annealing temperatures above 600 °C. The absence of mixing on the Ag/Pd and Ag/Fe interfaces and the fast migration of Pd atoms via a thick inert Ag buffer in the Fe film in the Pd/Ag/Fe trilayers prove the occurrence of LRCIs between Pd and Fe during the solid-state reaction. Our study takes an unprecedented look at the common nature of the LRCIs and chemical bonds.

**Acknowledgement**

The authors thank Dr L.A. Solovyov (Institute of Chemistry and Chemical Technology Russian Academy of Sciences) for assistance in the obtainment and analysis of XRD images.

## References

[1] A. Van der Ven, H.-C. Yu, G. Ceder and K. Thornton, Prog. Mater. Sci. 55 (2010) p.61.
[2] P. Heitjans and J. Kärger, *Diffusion in Condensed Matter: Methods, Materials, Models*, Springer, Berlin, 2005.
[3] J.M. Poate, K.N. Tu and J.W. Meyer (eds.), *Thin Films – Interdiffusion and Reaction*, Wiley-Interscience, New York, 1978.
[4] K.N. Tu, J.W. Mayer and L.C. Feldman, *Electronic Thin Film Science for Electrical Engineers and Materials Scientists*, Macmillan, New York, 1992.
[5] E.G. Colgan, Mater. Sci. Rep. 5 (1990) p.1.
[6] R. Pretorius, C.C. Theron, A. Vantomme and J.W. Mayer, Crit. Rev. Solid State Mater. Sci. 24 (1999) p.1.
[7] T. Laurila and J. Molarius, Crit. Rev. Solid State Mater. Sci. 28 (2003) p.185.
[8] A. Portavoce and G. Tréglia, Phys. Rev. B 82 (2010) p.205431.
[9] W.-H. Wang, H.Y. Bai, M. Zhang, J.H. Zhao, X.Y. Zhang and W.K. Wang, Phys. Rev. B 59 (1999) p.10811.
[10] N. Zotov, J. Feydt, A. Savan and A. Ludwig, J. Appl. Phys. 100 (2006) p.073517.
[11] V. Simić and Ž. Marinković, J. Mater. Sci. 33 (1998) p.561.
[12] L.A. Clevenger, B. Arcot, W. Ziegler, E.G. Colgan, Q.Z. Hong, F.M. d'Heurle, C. Cabral, T.A. Gallo and J.M.E. Harper, J. Appl. Phys. 83 (1998) p.90.
[13] B. Wang, D.C. Berry, Y. Chiari and K. Barmak, J. Appl. Phys. 110 (2011) p.013903.
[14] D. Mangelinck, K. Hoummada and I. Blum, Appl. Phys. Lett. 95 (2009) p.181902.
[15] Y.N. Picard and S.M. Yalisove, Appl. Phys. Lett. 92 (2008) p.014102.
[16] T. Höche, D. Ruthe and T. Petsch, Appl. Phys. A 79 (2004) p.961.
[17] F. Faupel, W. Frank, M.-P. Macht, H. Mehrer, V. Naundorf, K. Rätzke, H.R. Schober, S.K. Sharma and H. Teichler, Rev. Mod. Phys. 75 (2003) p.237.
[18] C.T. Wei, B.R. Maddox, A.K. Stover, T.P. Weihs, V.F. Nesterenko and M.A. Meyers, Acta Mater. 59 (2011) p.5276.
[19] J.M. Nawash, N.M. Masoud, K.A. Al-Saleh and N.S. Saleh, Appl. Phys. A 97 (2009) p.309.
[20] J.D.R. Buchanan, T.P.A. Hase, B.K. Tanner, P.J. Chen, L. Gan, C.J. Powell and W.F. Egelhoff Jr, Phys. Rev. B 66 (2002) p.104427.
[21] A.S. Rogachev, Russ. Chem. Rev. 77 (2008) p.21.
[22] S.S. Batsanov, Russ. Rev. 75 (2006) p.669.
[23] C.-D. Lien, M.-A Nicolet and C.S. Pai, J. Appl. Phys. 57 (1985) p.224.

[24] Q.Z. Hong and F.M. d'Heurle, J. Appl. Phys. 72 (1992) p.4036.
[25] C.M. Comrie and R.T. Newman, J. Appl. Phys. 79 (1996) p.153.
[26] K.S. Chi and L.J. Chen, J. Appl. Phys. 92 (2002) p.927.
[27] M.-A. Nicolet, Thin Solid Films 52 (1978) p.415.
[28] D.-S. Yoon, J.S. Roh, H.K. Baik and S.-M. Lee, Crit. Rev. Solid State Mater. Sci. 27 (2002) p.143.
[29] C. Detavernier C. Lavoie, F.M. d'Heurle, H. Bender and R.L. Van Meirhaeghe, J. Appl. Phys. 95 (2004) p.5340.
[30] Y. He, X.L. Liu, J.Y. Feng and Q.L. Wu, J. Appl. Phys. 96 (2004) p.6928.
[31] M. Lawrence, A. Dass, D.B. Fraser and C.S. Wei, Appl. Phys. Lett. 58 (1991) p.1308.
[32] C. Detavernier, R.L. Van Meirhaeghe, H. Bender, O. Richard, B. Brijs and K. Maex, J. Appl. Phys. 92 (2002) p.1207.
[33] H. Jeon, B. Jung, Y.D. Kim, W. Yang and R.J. Nemanich, J. Appl. Phys. 88 (2000) p.2467.
[34] C. Bechtold, J. Buschbeck, A. Lotnyk, B. Erkartal, S. Hamann, C. Zamponi, L. Schultz, A. Ludwig, L. Kienle, S. Fähler and E. Quandt, Adv. Mater. 22 (2010) p.2668.
[35] T. Ichitsubo, S. Takashima, E. Matsubara, Y. Tamada and T. Ono, Appl. Phys. Lett. 97 (2010) p.182508.
[36] K. Sato, K. Aoyagi and T.J. Konno, J. Appl. Phys. 107 (2010) p.024304.
[37] D.H. Wei and Y.D. Yao, Appl. Phys. Lett. 95 (2009) p.172503.
[38] S. Farjami, T. Fukuda and T. Kakeshita, J. Phys.: Conf. Ser. 165 (2009) p.012055.
[39] J. Lyubina, O. Gutfleisch and O. Isnard, J. Appl. Phys. 105 (2009) p.07A717.
[40] D. Pečko, K.Ž. Rožman, P.J. McGuiness, B. Pihlar and S. Kobe, J. Appl. Phys. 107 (2010) p.09A712.
[41] V.G. Myagkov, V.S. Zhigalov, L.E. Bykova, L.A. Solov'ev and G.N. Bondarenko, JETP Lett. 91 (2010) p.481.
[42] V.G. Myagkov, V.S. Zhigalov, B.A. Belyaev, L.E. Bykova, L.A. Solovyov and G.N. Bondarenko, J. Magn. Magn. Mater. 324 (2012) p.1571.
[43] O. Dugerjav, H. Kim and J.M. Seo, AIP Adv. 1 (2011) p.032156.
[44] A. Kovács, K. Sato and Y. Hirotsu, J. Appl. Phys. 102 (2007) p.123512.
[45] F. Chemam, K. Lenz and W. Kuch, Appl. Phys. A 92 (2008) p.381.
[46] F. Bisio, A. Toma, R. Moroni, R. Pasero, F.B. de Mongeot, C. Boragno, M. Canepa, U. Valbusa and L. Mattera, Phys. Rev. B 75 (2007) p.054407.
[47] J. Buschbeck, S. Hamann, A. Ludwig, B. Holzapfel, L. Schultz and S. Fähler, J. Appl. Phys. 107 (2010) p.113919.
[48] S. Farjami, T. Fukuda and T. Kakeshita, J. Phys.: Conf. Ser. 165 (2009) p.012055.
[49] H. Shima, K. Oikawa, A. Fujita, K. Fukamichi, K. Ishida and A. Sakuma, Phys. Rev. B 70 (2004) p.224408.
[50] D. Halley, B. Gilles, P. Bayle-Guillemaud, R. Arenal, A. Marty, G. Patrat and Y. Samson, Phys. Rev. B 70 (2004) p.174437.
[51] M. Ohtake, S. Ouchi, F. Kirino and M. Futamoto, J. Appl. Phys. 111 (2012) p.07A708.
[52] B. Bian, K. Sato, Y. Hirotsu and A. Makino, Appl. Phys. Lett. 75 (1999) p.3686.
[53] Q.-F. Zhan, S. Vandezande, K. Temst and C. Van Haesendonck, New J. Phys. 11 (2009) p.063003.
[54] G. Chen, J.X. Li, J. Zhu, J.H. Liang and Y.Z. Wu, J. Appl. Phys. 109 (2011) p.07C108.
[55] K. Noda, M. Higuchi, Y. Komaki, T. Tanaka, Y. Nozaki and K. Matsuyama, J. Phys.: Conf. Ser. 266 (2011) p.012014.
[56] R.M. Bozorth, *Ferromagnetism*, IEEE Press, New York, NY, 1978.
[57] H. Shima, K. Oikawa, A. Fujita, K. Fukamichi, K. Ishida and A. Sakuma, Phys. Rev. B 70 (2004) p.224408.
[58] D. Halley, P. Auric, P. Bayle-Guillemaud, B. Gilles, A. Marty and D. Jalabert, J. Appl. Phys. 91 (2002) p.9757.

[59] V. Gehanno, P. Auric, A. Marty and B. Gilles, J. Magn. Magn. Mater. 188 (1998) p.310.
[60] V.A. Tsurin, A.E. Ermakov, Yu.G. Lebedev and B.N. Filippov, Phys. Status Solidi A 33 (1976) p.325.
[61] D.G. Merkel, L. Bottyán, F. Tanczikó, Z. Zolnai, N. Nagy, G. Vértesy, J. Waizinger and L. Bommer, J. Appl. Phys. 109 (2011) p.124302.
[62] S.L. Zhang and J.R. Zhang, Phys. Status Solidi B 182 (1994) p.421.
[63] C. Boeglin, H. Bulou, J. Hommet, X. Le Cann, H. Magnan, P. Le Fèvre and D. Chandesris, Phys. Rev. B 60 (1999) p.4220.
[64] M. Liehr, H. Lefakis, F.K. LeGoues and G.W. Rubloff, Phys. Rev. B 33 (1986) p.5517.
[65] L. Ruan and D.M. Chen, Appl. Phys. Lett. 72 (1998) p.3464.
[66] V.G. Myagkov, V.S. Zhigalov, L.E. Bykova and G.N. Bondarenko, Int. J. SHS 18 (2009) p.117.
[67] V.G. Myagkov, O.A. Bayukov, L.E. Bykova, V.S. Zhigalov and G.N. Bondarenko, J. Exp. Theor. Phys. Lett. 80 (2004) p.487.
[68] R. Fischer and T.H. Fauster, Surf. Rev. Lett. 3 (1996) p.1783.
[69] J. Shu, B.P.A. Grandjean, E. Ghali and S. Kaliaguine, J. Membr. Sci. 77 (1993) p.181.
[70] V.G. Myagkov, V.C. Zhigalov, L.E. Bykova and G.N. Bondarenko, J. Magn. Magn. Mater. 305 (2006) p.534.
[71] K.N. Tu and B.S. Berry, J. Appl. Phys. 43 (1972) p.3283.
[72] P. Corni and G.M. Antonini, Phys. Status Solidi A 97 (1986) p.K21.
[73] P. Madakson and J. Karasinski, J. Appl. Phys. 67 (1990) p.6189.
[74] P. Madakson and J.C. Liu, J. Appl. Phys. 68 (1990) p.2121.
[75] P. Madakson, J. Appl. Phys. 70 (1991) p.1374.
[76] V.G. Myagkov, L.E. Bykova, G.N. Bondarenko, V.S. Zhigalov, A.I. Pol'skii and F.V. Myagkov, J. Exp. Theor. Phys. Lett. 71 (2000) p.183.
[77] C.S. Barrett and T.B. Massalski, *Structure of Metals*, 3rd ed., McGraw-Hill, New York, 1980.
[78] V.G. Myagkov, Y.N. Mikhlin, L.E. Bykova, V.K. Mal'tsev and G.N. Bondarenko, JETP Lett. 90 (2009) p.111.
[79] V.G. Myagkov, L.E. Bykova and G.N. Bondarenko, Dokl. Phys. 48 (2003) p.30.
[80] V.G. Myagkov, Dokl. Phys. 48 (2003) p.495.
[81] V.G. Myagkov, Y.L. Mikhlin, L.E. Bykova, G.V. Bondarenko and G.N. Bondarenko, Dokl. Phys. Chem. 431 (2010) p.52.
[82] H. Nakajima, JOM 49 (1997) p.15.
[83] A.A. Kodentsov, A. Paul, M.J.H. van Dal, C. Cserháti, A.M. Gusak and F.J.J. van Loo, Crit. Rev. Solid State Mater. Sci. 33 (2008) p.210.
[84] T.N. Narasimhan, Curr. Sci. 93 (2007) p.1257.
[85] V.G. Myagkov, L.E. Bykova, G.N. Bondarenko and G.V. Bondarenko, JETP Lett. 91 (2010) p.665.
[86] K.N. Tu, J. Appl. Phys. 43 (1972) p.1303.
[87] C.C. Chang and G. Quintana, Appl. Phys. Lett. 29 (1976) p.453.
[88] C.-A. Chang and G. Ottaviani, Appl. Phys. Lett. 44 (1984) p.901.
[89] W.E. Swartz Jr, J.H. Linn, J.M. Ammons and M.G. Kovac, Thin solid films 114 (1984) p.349.
[90] J.M. Guglielmacci and M. Gillet, Surf. Sci. 105 (1981) p.386.
[91] V.G. Myagkov, L.A. Li, L.E. Bykova, I.A. Turpanov, P.D. Kim, G.V. Bondarenko and G.N. Bondarenko, Phys. Solid State 42 (2000) p.968.
[92] V.G. Myagkov, L.E. Bykova and G.N. Bondarenko, Dokl. Phys. 48 (2003) p.206.
[93] V.G. Myagkov, V.S. Zhigalov, L.E. Bykova and G.N. Bondarenko, J. Magn. Magn. Mater. 305 (2009) p.534.

[94] V.G. Myagkov, O.A. Bayukov, L.E. Bykova and G.N. Bondarenko, J. Magn. Magn. Mater. 321 (2009) p.2260.
[95] V.G. Myagkov, L.E. Bykova, S.M. Zharkov and G.V. Bondarenko, Solid State Phenom. 138 (2008) p.377.
[96] G.I. Distler and V.G. Obronov, Nature 224 (1969) p.261.
[97] A.I. Ryabchikov, A.N. Didenko, E.V. Kozlov and Y.P. Sharkeev, Surf. Coat. Technol. 56 (1993) p.97.
[98] D.I. Tetelbaum, A.Y. Azov, E.V. Kuril'chik, V.Y. Bayankin, F.Z. Gilmutdinov and Y.A. Mendeleva, Vacuum 70 (2003) p.169.
[99] R. Di Leonardo, F. Saglimbeni and G. Ruocco, Phys. Rev. Lett. 100 (2008) p.106103.
[100] B. Pluis, T.N. Taylor, D. Frenkel and J.F. van der Veen, Phys. Rev. B 40 (1989) p.1353.
[101] N. Knorr, H. Brune, M. Epple, A. Hirstein, M.A. Schneider and K. Kern, Phys. Rev. B 65 (2002) p.115420.
[102] S.U. Nanayakkara, E.C.H. Sykes, L.C. Fernández-Torres, M.M. Blake and P.S. Weiss, Phys. Rev. Lett. 98 (2007) p.206108.
[103] R.H. French, V.A. Parsegian, R. Podgornik, R.F. Rajter, A. Jagota, J. Luo, D. Asthagiri, M.K. Chaudhury, Y.-M. Chiang, S. Granick, S. Kalinin, M. Kardar, R. Kjellander, D.C. Langreth, J. Lewis, S. Lustig, D. Wesolowski, J.S. Wettlaufer, W.-Y. Ching, M. Finnis, F. Houlihan, O.A. von Lilienfeld, C.J. van Oss and T. Zemb, Rev. Mod. Phys. 82 (2010) p.188.
[104] K.M. Jones, E. Tiesinga, P.D. Lett and P.S. Julienne, Rev. Mod. Phys. 78 (2006) p.483.
[105] J. Léonard, M. Walhout, A.P. Mosk, T. Müller, M. Leduc and C. Cohen-Tannoudji, Phys. Rev. Lett. 91 (2003) p.073203.
[106] P.F. Weck and N. Balakrishnan, Int. Rev. Phys. Chem. 25 (2006) p.283.
[107] F.J. DiSalvo, Science 247 (1990) p.649.
[108] L. Pauling, J. Chem. Edu. 69 (1992) p.519.
[109] G. Frenking and S. Shaik, J. Comput. Chem. 28 (2007) p.1.
[110] F. Weinhold and C.R. Landis, Science 316 (2007) p.61.
[111] H.S. Rzepa, Nat. Chem. 1 (2009) p.510.
[112] S.K. Lamoreaux, Phys. Rev. Lett. 78 (1997) p.5.
[113] C. Hertlein, L. Helden, A. Gambassi, S. Dietrich and C. Bechinger, Nature 451 (2008) p.172.
[114] P. Zuurbier, S. de Man, G. Gruca, K. Heeck and D. Iannuzzi, New J. Phys. 13 (2011) p.023027.
[115] J. Laurent, H. Sellier, A. Mosset, S. Huant and J. Chevrier, Phys. Rev. B 85 (2012) p.035426.
[116] G.L. Klimchitskaya, U. Mohideen and V.M. Mostepanenko, Rev. Mod. Phys. 81 (2009) p.1827.
[117] J.M. Obrecht, R.J. Wild, M. Antezza, L.P. Pitaevskii, S. Stringari and E.A. Cornell, Phys. Rev. Lett. 98 (2007) p.063201.
[118] D.M. Harber, J.M. Obrecht, J.M. McGuirk and E.A. Cornell, Phys. Rev. A 72 (2005) p.033610.
[119] H. Bender, PhW Courteille, C. Marzok, C. Zimmermann and S. Slama, Phys. Rev. Lett. 104 (2010) p.083201.